Inorg. Chem. **2005**, *44*, 6704–6716

Tuning of Redox Properties for the Design of Ruthenium Anticancer Drugs: Part 2. Syntheses, Crystal Structures, and Electrochemistry of Potentially Antitumor $[Ru^{III/II}Cl_{6-n}(Azole)_n]^z$ (n = 3, 4, 6) Complexes†

Erwin Reisner,‡,# Vladimir B. Arion,*,‡ Anna Eichinger,‡ Norbert Kandler,‡ Gerald Giester,§ Armando J. L. Pombeiro,*,# and Bernhard K. Keppler*,‡

Institute of Inorganic Chemistry−Bioinorganic, Environmental and Radiochemistry, University of Vienna, Währingerstr. 42, A-1090 Vienna, Austria, Centro de Química Estrutural, Complexo I, Instituto Superior Técnico, Av. Rovisco Pais, 1049−001 Lisbon, Portugal, and Institute of Mineralogy and Crystallography, University of Vienna, Althanstr. 14, A-1090 Vienna, Austria

Received March 11, 2005

A series of mixed chloro-azole ruthenium complexes with potential antitumor activity, viz., *mer*-$[Ru^{III}Cl_3(azole)_3]$ (**B**), *trans*-$[Ru^{III}Cl_2(azole)_4]Cl$ (**C**), *trans*-$[Ru^{II}Cl_2(azole)_4]$ (**D**), and $[Ru^{II}(azole)_6](SO_3CF_3)_2$ (**E**), where azole = 1-butylimidazole (**1**), imidazole (**2**), benzimidazole (**3**), 1-methyl-1,2,4-triazole (**4**), 4-methylpyrazole (**5**), 1,2,4-triazole (**6**), pyrazole (**7**), and indazole (**8**), have been prepared as a further development of anticancer drugs with the general formula $[RuCl_4(azole)_2]^-$ (**A**). These compounds were characterized by elemental analysis, IR spectroscopy, electronic spectra, electrospray mass spectrometry, and X-ray crystallography. The electrochemical behavior has been studied in detail in DMF, DMSO, and aqueous media using cyclic voltammetry, square wave voltammetry, and controlled potential electrolysis. Compounds **B** and a number of **C** complexes exhibit one Ru^{III}/Ru^{II} reduction, followed, at a sufficiently long time scale, by metal dechlorination on solvolysis. The redox potential values in organic media agree with those predicted by Lever's parametrization method, and the yet unknown E_L parameters were estimated for **1** (E_L = 0.06 V), **3** (E_L = 0.10 V), **4** (E_L = 0.17 V), and **5** (E_L = 0.18 V). The E_L values for the azole ligands **1**–**8** correlate linearly with their basicity (pK_a value of the corresponding azolium acid H_2L^+). In addition, a logarithmic dependence between the homogeneous rate constants for the reductively induced stepwise replacement of chloro ligands by solvent molecules and the Ru^{III}/Ru^{II} redox potentials was observed. Lower $E_{1/2}$ values (higher net electron donor character of the ligands) result in enhanced kinetic rate constants of solvolysis upon reduction. The effect of the net charge on the Ru^{III}/Ru^{II} redox potentials in water is tentatively explained by the application of the Born equation. In addition, the pH-dependent electrochemical behavior of *trans*-$[RuCl_2(1,2,4\text{-triazole})_4]Cl$ is discussed.

Introduction

Ruthenium(III) complexes with the general formula $(HL)[RuCl_4L_2]$ (L = azole heterocycle) are well-known for their antitumor properties.[1] Different activities for the two geometrical isomers of $[RuCl_4(Htrz)_2]^-$ (Htrz = 1,2,4-triazole) were reported: the trans species exhibits higher antiproliferative activity than the cis complex in three human carcinoma cell lines (SW480, HT29, and SK-BR-3).[2] From a number of $(HL)[trans\text{-}Ru^{III}Cl_4L_2]$ compounds (**A**) with different azole ligands, the indazole complex shows the most

* To whom correspondence should be addressed. E-mail: arion@ap.univie.ac.at (V.B.A.); pombeiro@ist.utl.pt (A.J.L.P.); keppler@ap.univie.ac.at (B.K.K.). Fax: +43 1 4277 52680.

† Part 1: see ref 6.

‡ Institute of Inorganic Chemistry−Bioinorganic, Environmental and Radiochemistry, University of Vienna.

Centro de Química Estrutural, Complexo I, Instituto Superior Técnico.

§ Institute of Mineralogy and Crystallography, University of Vienna.

(1) (a) Clarke, M. J. *Coord. Chem. Rev.* **2003**, *236*, 209−233 and references therein. (b) Clarke, M. J.; Zhu, F.; Frasca, D. R. *Chem. Rev.* **1999**, *99*, 2511−2533 and references therein. (c) Galanski, M.; Arion, V. B.; Jakupec, M. A.; Keppler, B. K. *Curr. Pharm. Des.* **2003**, *9*, 2078−2089. (d) Keppler, B. K.; Lipponer, K. G.; Stenzel, B.; Kratz, F. New Tumor-Inhibiting Ruthenium Complexes. In *Metal Complexes in Cancer Chemotherapy*; Keppler, B. K., Ed.; VCH: Weinheim, Germany, 1993; pp 187−220. (e) Pieper, T.; Borsky, K.; Keppler, B. K. *Top. Biol. Inorg. Chem.* **1999**, *1*, 171−199.

(2) Arion, V. B.; Reisner, E.; Fremuth, M.; Jakupec, M. A.; Keppler, B. K.; Kukushkin, V. Yu.; Pombeiro, A. J. L. *Inorg. Chem.* **2003**, *42*, 6024−6031.

10.1021/ic0503737 CCC: $30.25
Published on Web 08/17/2005

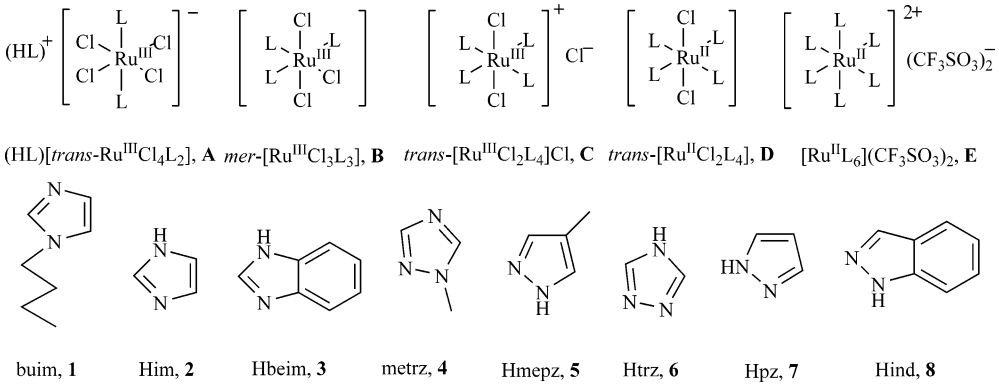

Figure 1. Types (**A**−**E**) of ruthenium complexes and their azole (L) ligands (**1**−**8**).

promising antitumor properties. Thus, (H$_2$ind)[*trans*-Ru^{III}Cl$_4$(Hind)$_2$] (KP1019, Hind = indazole) has been selected for clinical trials in 2003 because of its remarkable activity against autochthonous colorectal carcinoma.[1c−e,3]

Although the antiproliferative activity of the (HL)[*trans*-RuCl$_4$L$_2$] complexes has been known since 1986,[4] the mode of antitumor action is not yet understood, at least, at the molecular level. The activation of such ruthenium prodrugs by reduction[5−7] is a plausible pathway because the complexes possess a biologically accessible Ru^{III}/Ru^{II} redox potential (e.g., $E_{1/2}$, Na[*trans*-RuCl$_4$(Hind)$_2$] = +0.03 V vs NHE in 0.2 M phosphate buffer at pH 7.0).[6] Glutathione and ascorbic acid were shown to reduce *trans*-[RuCl$_4$(Hind)$_2$]$^-$ under physiological conditions,[8] and the resulting Ru^{II} species is supposed to coordinate readily to biomolecules.[1a] Investigations of the redox potentials and antiproliferative activity for KP1019 derivatives support the "activation by reduction" hypothesis, and the increase of Ru^{III}/Ru^{II} redox potentials correlates with an enhanced cytotoxic potency on SW-480 (colon carcinoma) cell line as follows: [Ru^{III}Cl$_4$(Him)$_2$]$^-$ (Him = imidazole) < [Ru^{III}Cl$_4$(Htrz)$_2$]$^-$ < [Ru^{III}Cl$_4$(Hind)$_2$]$^-$ < [Ru^{III}Cl$_3$(Hind)$_3$] < [Ru^{III}Cl$_2$(Hind)$_4$]$^+$ ≈ [Ru^{II}Cl$_2$(Hind)$_4$].[2,6,9]

The cytotoxicity and DNA binding of the anticancer agent (H$_2$im)[*trans*-RuCl$_4$(Him)$_2$] was shown to increase with a concomitant decrease of the O_2 partial pressure,[10] in accordance with a reductively induced activation of the Ru^{III} prodrugs in the hypoxic tumor tissue. The recently reported crystallographic evidence for coordination of 9-methyladenine and thioethers to *trans*-[RuCl$_4$(Hind)$_2$]$^-$ suggests that both DNA and S-containing biological molecules are possible targets for such metallo(pro)drugs.[11]

In addition, homoleptic azole-based ruthenium(II) complexes of the type [Ru(azole)$_6$]$^{2+}$ are currently under investigations because of their good pharmacological properties as radiosensitizers.[12,13] Therefore, we have prepared a variety of azole-based ruthenium complexes (some of them dissolve well in water), which allowed the establishment of useful structure−property relationships for future drug development.

Herein, we report on (i) the synthesis of a series of *mer*-[Ru^{III}Cl$_3$L$_3$] (**B**), *trans*-[Ru^{III}Cl$_2$L$_4$]Cl (**C**), *trans*-[Ru^{II}Cl$_2$L$_4$] (**D**), and [Ru^{II}L$_6$](CF$_3$SO$_3$)$_2$ (**E**) complexes using the azole ligands 1-butylimidazole (buim, **1**), imidazole (Him, **2**), benzimidazole (Hbeim, **3**), 1-methyl-1,2,4-triazole (metrz, **4**), 4-methylpyrazole (Hmepz, **5**), 1,2,4-triazole (Htrz, **6**), pyrazole (Hpz, **7**), and indazole (Hind, **8**), (ii) the structural characterization of a number of such complexes, and (iii) a methodological electrochemical study of **A**−**E** (Figure 1).

Experimental Section

Physical Measurements. Elemental analyses, IR spectroscopy, and ESI mass spectroscopy measurements were carried out as described previously.[6] The electronic spectra were obtained with a Perkin-Elmer Lambda 20 UV−vis spectrophotometer using samples dissolved in methanol or 0.2 M phosphate buffer. The ^{1}H NMR spectra were recorded at 400.13 MHz on a Bruker DPX400 spectrometer at 298 K. The chemical shifts for ^{1}H were referenced to residual ^{1}H present in deuterated dimethyl sulfoxide. The pH values were determined with an Eco-Scan pH meter.

Electrochemistry. The electrochemical measurements were carried out as reported previously.[6] For cyclic voltammetry (CV), a 0.5 mm diameter platinum disk (for **B**−**E**) and a 1.0 mm diameter glassy-carbon disk (for **A**) were used as working electrodes. The latter was applied to avoid the protic reduction of the azolium counterion. The potentials were measured in 0.15 M [*n*-Bu$_4$N][BF$_4$]/DMF or DMSO using [Fe(η^5-C$_5$H$_5$)$_2$] ($E_{1/2}$ = +0.72 V or +0.68 V vs NHE in DMF or DMSO, respectively)[14] as internal standards. The redox potentials measured in the 0.2 M phosphate buffer were

(3) Berger, M. R.; Garzon, F. T.; Keppler, B. K.; Schmähl, D. *Anticancer Res.* **1989**, *9*, 761−765.
(4) Keppler, B. K.; Rupp, W. *J. Cancer Res. Clin. Oncol.* **1986**, *111*, 166−168.
(5) Clarke, M. J. In *Metal Ions in Biological Systems*, Vol. 11; H. Sigel, Ed.; Marcel Dekker: New York, 1980; p 231.
(6) Reisner, E.; Arion, V. B.; Guedes da Silva, M. F. C.; Lichtenecker, R.; Eichinger, A.; Keppler, B. K.; Kukushkin, V. Yu.; Pombeiro, A. J. L. *Inorg. Chem.* **2004**, *43*, 7083−7093.
(7) Alessio, E.; Balducci, G.; Lutman, A.; Mestroni, G.; Calligaris, M.; Attia, W. *Inorg. Chim. Acta* **1993**, *203*, 205−217.
(8) Schluga, P.; Hartinger, Ch.; Egger, A.; Reisner, E.; Galanski, M.; Jakupec, M.; Keppler, B. K. Manuscript in preparation.
(9) Jakupec, M. A.; Reisner, E.; Eichinger, A.; Pongratz, M.; Arion, V. B.; Galanski, M.; Hartinger, Ch.; Keppler, B. K. *J. Med. Chem.* **2005**, *48*, 2831−2837.
(10) Frasca, D.; Ciampa, J.; Emerson, J.; Umans, R. S.; Clarke, M. J. *Metal-Based Drugs* **1996**, *3*, 197−209.
(11) Egger, A.; Arion, V. B.; Reisner, E.; Cebrián-Losantos, B.; Shova, S.; Trettenhahn, G.; Keppler, B. K. *Inorg. Chem.* **2005**, *44*, 122−132.
(12) Bastos, C. M.; Gordon, K. A.; Ocain, T. D. *Bioorg. Med. Chem. Lett.* **1998**, *8*, 147−150.
(13) Newcomb, J. R.; Rivnay, B.; Bastos, C. M.; Ocain, T. D.; Gordon, K.; Gregory, P.; Turci, S. M.; Sterne, K. A.; Jesson, M.; Krieger, J.; Jenson, J. C.; Jones, B. *Inflamm. Res.* **2003**, *52*, 263−271.
(14) Barette, W. C., Jr.; Johnson, H. W., Jr.; Sawyer, D. T. *Anal. Chem.* **1984**, *56*, 1890−1898.

Table 1. Crystal Data and Details of Data Collection for **B1**, **B4**, **B5**, **B6**·H_2O, and **B7**

	B1	**B4**	**B5**	**B6**·H_2O	**B7**
chemical formula	$C_{21}H_{36}N_6Cl_3Ru$	$C_9H_{15}N_9Cl_3Ru$	$C_{12}H_{18}N_6Cl_3Ru$	$C_6H_{11}N_9Cl_3ORu$	$C_9H_{12}N_6Cl_3Ru$
fw	579.98	456.70	453.74	432.64	411.66
space group	$P2_1/c$	$P2_1/n$	$P2_12_12_1$	$P2_1/c$	$P2_1/n$
a (Å)	17.730(4)	7.139(1)	11.313(2)	8.1046(16)	18.936(4)
b (Å)	10.794(2)	19.878(4)	11.546(2)	14.693(3)	8.028(2)
c (Å)	27.802(6)	12.167(2)	13.456(3)	11.754(2)	19.180(4)
β (deg)	90.35(3)	92.62(3)		98.29(3)	91.64(3)
V (Å^3)	5320.6(19)	1724.8(5)	1757.6(6)	1385.1(5)	2914.5(11)
Z	8	4	4	4	8
d_{calcd} (g cm^{-3})	1.448	1.759	1.715	2.075	1.876
μ (cm^{-1})	9.11	13.83	13.52	17.21	16.20
T (K)	120	120	120	120	298
R1[a]	0.0310	0.0291	0.0200	0.0243	0.0314
wR2[b]	0.0959	0.0720	0.0451	0.0545	0.0697

[a] $R1 = \sum||F_o| - |F_c||/\sum|F_o|$. [b] $wR2 = \{\sum[w(F_o^2 - F_c^2)^2]/\sum[w(F_o^2)^2]\}^{1/2}$.

Table 2. Crystal Data and Details of Data Collection for **C2**, **C3**·MeOH·Et_2O, **C6a**·$2H_2O$, **C7**, and **E4b**

	C2	**C3**·MeOH·Et_2O	**C6a**·$2H_2O$	**C7**	**E4b**
chemical formula	$C_{12}H_{16}N_8Cl_3Ru$	$C_{33}H_{38}N_8Cl_3O_2Ru$	$C_8H_{16}N_{12}Cl_2F_6O_2RuSb$	$C_{12}H_{16}N_8Cl_3Ru$	$C_{18}H_{30}N_{18}B_2F_8Ru$
fw	479.74	786.13	720.05	479.74	773.23
space group	$C2/c$	$P2_1/n$	$P\bar{1}$	$P\bar{1}$	$R\bar{3}$
a (Å)	9.6322(19)	15.748(3)	7.4500(15)	7.9169(16)	12.194(2)
b (Å)	18.979(4)	13.699(3)	7.6149(15)	8.4136(17)	
c (Å)	9.6991(19)	16.564(3)	10.550(2)	14.658(3)	17.336(3)
α (deg)			81.82(3)	102.90(3)	
β (deg)	90.01(3)	93.66(3)	88.66(3)	90.93(3)	
γ (deg)			63.26(3)	110.60(3)	
V (Å^3)	1773.1(6)	3566.1(12)	528.51(18)	886.0(3)	2232.4(6)
Z	4	4	1	2	3
d_{calcd} (g cm^{-3})	1.797	1.464	2.262	1.798	1.726
μ (cm^{-1})	13.49	7.07	23.32	13.50	6.24
T (K)	120	120	120	120	120
R1[a]	0.0186	0.0302	0.0432	0.0257	0.0345
wR2[b]	0.0449	0.0871	0.1206	0.0559	0.0886

[a] $R1 = \sum||F_o| - |F_c||/\sum|F_o|$. [b] $wR2 = \{\sum[w(F_o^2 - F_c^2)^2]/\sum[w(F_o^2)^2]\}^{1/2}$.

first examined by CV to confirm the reversibility of each couple and then measured by square wave voltammetry (2 mV step height, 25 mV pulse, 100 Hz frequency) using a 0.2 mm diameter carbon disk working electrode and a Ag/AgCl reference electrode. The pH value of the electrolyte solution was controlled before and after the measurement for constancy. The single-electron transfer for the Ru^{III}/Ru^{II} redox couple has been confirmed by coulometric measurements (consumption of one mol equivalent of electrons). All potentials are quoted relative to the normal hydrogen electrode (NHE).

Crystallographic Structure Determination. X-ray diffraction measurements were performed on a Nonius Kappa CCD diffractometer with Mo K_α radiation ($\lambda = 0.71073$ Å). Single crystals were positioned at 40, 30, 30, 30, 30, 30, 30, 30, 30, and 30 mm from the detector, and 845, 419, 261, 341, 702, 376, 341, 376, 376, and 295 frames were measured, each for 55, 35, 150, 25, 20, 25, 25, 145, 75, and 120 s over a 1, 1.5, 2, 2, 1, 2, 2, 2, 2, and 2° angle for **B1**, **B4**, **B5**, **B6**·H_2O, **B7**, **C2**, **C3**·CH_3OH·$(C_2H_5)_2O$, **C6a**·$2H_2O$, **C7**, and **E4**, respectively. The data were processed using the Denzo-SMN software. The structures were solved by direct methods using the SHELXS-97 program and refined by full-matrix least-squares techniques with SHELXL-97.[15] All hydrogens were inserted in calculated positions and refined using a riding model. Drawings were made with ORTEP.[16] Crystal data, data collection parameters, and structure refinement details for **B** are given in Table 1 and for **C** and **E** in Table 2.

Chemicals. Hydrated $RuCl_3$ was purchased from Degussa; 1-butylimidazole and 4-methylpyrazole were purchased from Acros, and imidazole and indazole from Sigma-Aldrich. Benzimidazole, 1*H*-1,2,4-triazole, and pyrazole were from Fluka, and 1-methyl-1,2,4-triazole was from Lancaster. All of these chemicals were used as received.

Synthesis of the Complexes. $(Et_4N)_2[Ru_2Cl_7(OH)_3]$·HCl,[17] $(NEt_4)[RuCl_4(MeCN)_2]$,[17] *trans*-$[RuCl_2(MeCN)_4]$,[18] $[RuCl_3(PhSEt)_3]$,[19] $[Ru(CH_3CN)_6](ZnCl_4)_2$·$2.55H_2O$,[20] $[Ru(DMF)_6](SO_3CF_3)_3$,[21] [Ru-(1,5-cyclooctadiene)$(MeCN)_4$]$(BF_4)_2$,[22] (H_2pz)[*trans*-$RuCl_4(Hpz)_2$] (**A7**),[23] (H_2ind)[*trans*-$RuCl_4(Hind)_2$] (**A8**),[24] *mer*-$[RuCl_3(Hind)_3]$

(15) (a) Sheldrick, G. M. *SHELXS-97, Program for Crystal Structure Solution*: University Göttingen: Göttingen, Germany, 1997. (b) Sheldrick, G. M. *SHELXL-97, Program for Crystal Structure Refinement*: University Göttingen: Göttingen, Germany, 1997.

(16) (a) Johnson, C. K. Report ORNL-5138; OAK Ridge National Laboratory: OAK Ridge, TN, 1976. (b) *International Tables for X-ray Crystallography*; Kluwer Academic Press: Dordrecht, The Netherlands, 1992; Vol. C, Tables 4.2.6.8 and 6.1.1.4.

(17) Braunstein, P.; Rose, J. *Inorg. Synth.* **1989**, *26*, 356−360

(18) Johnson, B. F. G.; Lewis, J.; Ryder, I. E. *J. Chem. Soc., Dalton Trans.* **1977**, 719−724.

(19) Chatt, J.; Leigh, G. J.; Storace, A. P. *J. Chem. Soc. A* **1971**, 1380−1389.

(20) Anzellotti, A.; Briceño, A. *Acta Crystallogr.* **2001**, *E57*, m538−m540.

(21) Judd, R. J.; Renhai, C.; Biner, M.; Armbruster, T.; Bürgi, H.-B.; Merbach, A. E.; Ludi, A. *Inorg. Chem.* **1995**, *34*, 5080−5083.

(22) Widegren, J. A.; Weiner, H.; Miller, S. M.; Finke, R. G. *J. Organomet. Chem.* **2000**, *610*, 112−117.

(23) Juhl, U. M. Ph.D. Thesis, University of Heidelberg, Heidelberg, Germany, 1987.

(24) Lipponer, K. G.; Vogel, E.; Keppler, B. K. *Metal-Based Drugs* **1996**, *3*, 243−260.

(**B8**),[25] *trans*-[$RuCl_2(Hind)_4$]Cl (**C8**),[9] *trans*-[$RuCl_2(Hind)_4$] (**D8**),[9] and [$Ru(Him)_6$](SO_3CF_3)$_2$[12] were prepared as described elsewhere.

(H_2beim)[*trans*-$Ru^{III}Cl_4(Hbeim)_2$]·$^1/_2H_2O$ (A3). A "diluted Kralik solution" of "$RuCl_3$" (10 mL, 2.8 mmol), prepared as described in the literature,[26] was added to a hot solution (80 °C) of benzimidazole (3.36 g, 28.4 mmol) in 1 M HCl (10 mL). The reaction mixture was refluxed for 5 min and allowed to cool to room temperature. The wine-red solid precipitated was filtered off after it stood at room temperature for 4 days; it was then washed with ethanol and diethyl ether and dried at room temperature in vacuo. Yield: 1.48 g, 87%. Anal. Calcd for $C_{21}H_{20}N_6Cl_4O_{0.5}Ru$ (M_r = 607.3 g/mol): C, 41.53; H, 3.32; N, 13.84; Cl, 23.35. Found: C, 41.73; H, 3.37; N, 13.90; Cl, 23.12. ESI-MS (negative): *m*/*z* 480 [$RuCl_4(Hbeim)_2$]$^-$. IR spectrum in KBr, selected bands: 3284 s, br ν(O−H), 1490 s, 1408 s, 1245 s, 731 vs, 589 s, 420 s cm^{-1}. UV−vis (MeOH), λ_{max} (ϵ): 404 (1.28), 351 nm (3.17 mM^{-1} cm^{-1}).

***mer*-[$Ru^{III}Cl_3(buim)_3$] (B1).** 1-Butylimidazole (2.50 g, 20.2 mmol) was added to a solution of [$RuCl_3(PhSEt)_3$] (1.40 g, 2.2 mmol) in toluene (45 mL). The mixture was refluxed for 4 h, then left to cool to room temperature, and allowed to stand at 4 °C overnight. The solid formed was filtered off and redissolved in a minimum amount of acetone (ca. 5 mL). The addition of diethyl ether (ca. 8 mL) produced yellow microcrystals, which were filtered off, washed with diethyl ether, and dried at room temperature in air. Yield: 0.70 g, 55%. Anal. Calcd for $C_{21}H_{36}N_6Cl_3Ru$ (M_r = 579.98 g/mol): C, 43.49; H, 6.26; N, 14.49; Cl, 18.34. Found: C, 43.59; H, 6.54; N, 14.48; Cl, 18.09. ESI-MS (negative): *m*/*z* 616, [$RuCl_3(buim)_3$+Cl]$^-$. ESI-MS (positive): *m*/*z* 604, [$RuCl_3(buim)_3$+Na]$^+$. IR spectrum in KBr, selected bands: 3124 s, 3108 s, 2956 s, 2928 s, 1516 s, 1099 vs, 827 s, 623 s cm^{-1}. UV−vis (MeOH), λ_{max} (ϵ): 393 (1.10), 347 (3.29), 282 nm (1.71 mM^{-1} cm^{-1}). Suitable crystals for the X-ray diffraction study were selected directly from the reaction vessel.

***mer*-[$Ru^{III}Cl_3(Hbeim)_3$] (B3).** A mixture of (H_2beim)[*trans*-$Ru^{III}Cl_4(Hbeim)_2$]·$^1/_2H_2O$ (**A3**) (1.48 g, 2.4 mmol) and benzimidazole (0.38 g, 3.2 mmol) in ethanol/water (100 mL, 7:3) was refluxed for 2 h. When the solution was cooled to room temperature, it deposited an orange product, which was consequently recrystallized from ethyl acetate and acetone and dried at 200 °C under argon. Yield: 0.43 g, 31%. Anal. Calcd for $C_{21}H_{18}N_6Cl_3Ru$ (M_r = 561.84 g/mol): C, 44.89; H, 3.23; N, 14.96; Cl, 18.93. Found: C, 44.64; H, 3.21; N, 14.80; Cl, 18.48. ESI-MS (negative): *m*/*z* 562 [$RuCl_3$(beim)($Hbeim)_2$]$^-$. IR spectrum in KBr, selected bands: 3275 vs, 1414 s, 1303 s, 1247 s, 748 vs cm^{-1}. UV−vis (MeOH), λ_{max} (ϵ): 411 (2.18), 358 (3.12), 278 (18.44), 270 nm (19.29 mM^{-1} cm^{-1}).

***mer*-[$Ru^{III}Cl_3(metrz)_3$] (B4).** (NEt_4)[$RuCl_4(MeCN)_2$] (0.15 g, 0.33 mmol) was added to 1-methyl-1,2,4-triazole (0.5 mL) at 125 °C. The dark-red mixture, which turned orange-red after 0.25 h, was heated for 1 h and allowed to cool to room temperature. The red crystals formed after 3 weeks were filtered off, washed with ethanol and diethyl ether, and dried at room temperature in vacuo. Yield: 0.07 g, 46%. Anal. Calcd. for $C_9H_{15}N_9Cl_3Ru$ (M_r = 456.70 g/mol): C, 23.67; H, 3.31; N, 27.60; Cl, 23.29. Found: C, 23.84; H, 3.07; N, 27.57; Cl, 22.84. ESI-MS (negative): *m*/*z* 493 [$RuCl_3$-$(metrz)_3$ + Cl]$^-$, 410 [$RuCl_3(metrz)_2$ + Cl]$^-$. ESI-MS (positive): *m*/*z* 481 [$RuCl_3(metrz)_3$ + Na]$^+$. IR spectrum in KBr, selected bands: 3143 s, 1539 vs, 1292 vs, 1121 vs, 996 vs, 877 vs, 697 vs, 677 vs cm^{-1}. UV−vis (MeOH), λ_{max} (ϵ): 418 (1.05), 371 nm (3.55, mM^{-1} cm^{-1}). Red crystals suitable for the X-ray diffraction study were selected directly from the reaction vessel.

***mer*-[$Ru^{III}Cl_3(Hmepz)_3$] (B5).** A solution of (H_2mepz)[*trans*-$RuCl_4(Hmepz)_2$] (**A5**) (0.52 g, 1.1 mmol) and 4-methylpyrazole (0.21 g, 2.6 mmol) in ethanol/water (20 mL, 7:3) was refluxed for 2 h. The orange-red solid deposited when the reaction mixture was cooled to room temperature was filtered off, washed with water, and dried in a desiccator over P_4O_{10}. Yield: 0.17 g, 35%. Anal. Calcd for $C_{12}H_{18}N_6Cl_3Ru$ (M_r = 453.74 g/mol): C, 31.77; H, 4.00; N, 18.52; Cl, 23.44. Found: C, 32.06; H, 4.06; N, 18.21; Cl, 23.34. ESI-MS (negative): *m*/*z* 454 [$RuCl_3(Hmepz)_2$(mepz)]$^-$. IR spectrum in KBr, selected bands: 3280 s, 1114 vs, 1070 vs, 1002 vs, 837 s, 607 s, 600 s, 590 s cm^{-1}. UV−vis (MeOH), λ_{max} (ϵ): 398 (2.98), 369 nm (3.08 mM^{-1} cm^{-1}). Single crystals suitable for the X-ray diffraction study were obtained from a solution of **B5** in ethanol/water (7:3) at 4 °C.

***mer*-[$Ru^{III}Cl_3(Htrz)_3$]·H_2O (B6·H_2O).** Finely ground $(Et_4N)_2$-[$Ru_2Cl_7(OH)_3$]·HCl (0.60 g, 0.76 mmol) was dissolved in aqueous HCl (1 M, 100 mL) at room temperature under ultrasound treatment (ca. 20 min). 1*H*,2,4-Triazole (6.00 g, 86.87 mmol) was added to this solution, and the suspension treated with ultrasound for ca. 5 min. The dark-green solution was filtered to remove the undissolved material and allowed to stand at room temperature. Red-brown plates of the product contaminated by amorphous impurities were filtered off after 4 weeks. The treatment of the crude product with ethanol (3 × 5 mL) in an ultrasonic bath (ca. 30 s) allowed us to remove the dissolved impurities by filtration. The remaining brown plates were washed with diethyl ether and dried at room temperature in air. Yield: 0.23 g, 35%. Anal. Calcd. for $C_6H_{11}N_9Cl_3ORu$ (M_r = 432.64 g/mol): C, 16.66; H, 2.56; N, 29.14; Cl, 24.58. Found: C, 16.69; H, 2.60; N, 28.82; Cl, 24.30. ESI-MS (negative): *m*/*z* 415 [$RuCl_3(Htrz)_2$(trz)]$^-$, 346 [$RuCl_3(Htrz)$(trz)]$^-$, 277 [$RuCl_3$(trz)]$^-$. IR spectrum in KBr, selected bands: 3120 s, 1518 s, 1411 s, 1301 s, 1050 s, 871 s, 842 s, 621 vs cm^{-1}. UV−vis (MeOH), λ_{max} (ϵ): 427 (1.01), 376 nm (3.35 mM^{-1} cm^{-1}). Single crystals suitable for the X-ray diffraction study were picked out directly from the reaction vessel.

***mer*-[$Ru^{III}Cl_3(Hpz)_3$] (B7).** A solution of (H_2pz)[*trans*-$RuCl_4$-$(Hpz)_2$] (**A7**) (6.70 g, 15.0 mmol) and pyrazole (1.00 g, 14.7 mmol) in ethanol/water (250 mL, 7:3) was refluxed for 5 h, then cooled to room temperature, and reduced in volume until a precipitate had started to form. The solid was filtered off and washed with water and ethanol. Recrystallization by vapor diffusion of diethyl ether into a methanol solution (200 mL) of the complex gave red crystals, which were filtered off, washed with water (2 × 2 mL), and dried in a desiccator over P_4O_{10}. Yield: 0.17 g, 3%. Anal. Calcd for $C_9H_{12}N_6Cl_3Ru$ (M_r = 411.66 g/mol): C, 26.26; H, 2.94; N, 20.42; Cl, 25.84. Found: C, 26.53; H, 2.77; N, 20.24; Cl, 25.47. ESI-MS (negative): *m*/*z* 412, [$RuCl_3$(pz)($Hpz)_2$]$^-$. IR spectrum in KBr, selected bands: 3346 s, 1470 s, 1346 s, 1117 vs, 1044 vs, 908 s, 763 vs cm^{-1}. UV−vis (MeOH), λ_{max} (ϵ): 376 nm (3.18 mM^{-1} cm^{-1}). X-ray diffraction quality single crystals were obtained by vapor diffusion of diethyl ether into a methanol solution of the complex.

***trans*-[$Ru^{III}Cl_2(Him)_4$]Cl (C2).** A solution of freshly prepared [$RuCl_3(EtSPh)_3$] (2.00 g, 3.2 mmol) in toluene (125 mL) was added to a solution of imidazole (2.00 g, 29.4 mmol) in ethanol (20 mL), and the reaction mixture was refluxed for 0.5 h. The black precipitate formed was separated by filtration, suspended in hot $CHCl_3$ (25 mL), treated with ultrasound, and filtered off again. This operation was repeated three times. The crude product (1.40 g) was redissolved in methanol (40 mL), and the solution filtered to remove

(25) Pieper, T.; Sommer, M.; Galanski, M.; Keppler, B. K.; Giester, G. *Z. Anorg. Allg. Chem.* **2001**, *627*, 261−265.
(26) Kralik, F.; Vrestal, J. *Collect. Czech. Chem. Commun.* **1961**, *26*, 1298−1304.

the undissolved material. Diethyl ether was added to the filtered solution until a green precipitate had started to form. The solution was filtered again and reduced in volume depositing a solid, which was filtered off, washed with diethyl ether, and dried at room temperature in air. Yield: 0.66 g, 43%. Anal. Calcd for $C_{12}H_{16}N_8Cl_3Ru$ (M_r = 479.74 g/mol): C, 30.04; H, 3.36; N, 23.36; Cl, 22.17. Found: C, 29.71; H, 3.15; N, 23.33; Cl, 21.44. ESI-MS (positive): *m*/*z* 444 $[RuCl_2(Him)_4]^+$. IR spectrum in KBr, selected bands: 3143 s, 1332 s, 1074 vs, 771 s, 742 vs, 729 vs, 656 vs, 616 vs cm^{-1}. UV−vis (MeOH), λ_{max} (ϵ): 346 (2.71), 275 nm (1.31, mM^{-1} cm^{-1}). Solubility in water at 298 K: 9 mg/mL. Crystals suitable for the X-ray diffraction study were obtained by vapor diffusion of diethyl ether into a methanol solution of the complex.

***trans*-[$Ru^{III}Cl_2$(Hbeim)$_4$]Cl (C3).** A solution of (Hbeim)[*trans*-$Ru^{III}Cl_4$(Hbeim)$_2$]·$^1/_2H_2O$ (**A3**) (0.13 g, 0.21 mmol) and benzimidazole (0.04 g, 0.34 mmol) in ethanol/water (50 mL, 7:3) was refluxed for 4 h and allowed to stand overnight at room temperature. The solution volume was reduced to ca. 10 mL to give a solid, which was filtered off and recrystallized first from ethyl acetate and then from acetone. The orange powder was dried at 200 °C under argon. Yield: 0.10 g, 69%. Anal. Calcd for $C_{28}H_{24}N_8Cl_3Ru$ (M_r = 679.97 g/mol): C, 49.46; H, 3.56; N, 16.48; Cl, 15.64. Found: C, 49.40; H, 3.31; N, 16.19; Cl, 15.41. ESI-MS (positive): *m*/*z* 644 $[RuCl_2(Hbeim)_4]^+$. IR spectrum in KBr, selected bands: 3129 s, 1507 s, 1494 s, 1421 s, 1264 s, 739 vs, 455 s cm^{-1}. UV−vis (MeOH), λ_{max} (ϵ): 363 nm (2.67 mM^{-1} cm^{-1}). Crystals of *trans*-$[RuCl_2(Hbeim)_4]Cl·MeOH·Et_2O$ (**C3**·MeOH·Et_2O) suitable for the X-ray diffraction study were obtained by vapor diffusion of diethyl ether into a methanol solution of **C3**.

***trans*-[$Ru^{III}Cl_2$(Htrz)$_4$]Cl (C6).** *mer*-$[RuCl_3(Htrz)_3]·H_2O$ (**B6**) (0.20 g, 0.46 mmol) was added to the molten 1*H*,2,4-triazole (0.70 g, 10.14 mmol), and the reaction mixture heated at 130 °C for 0.75 h. The molten mass turned from dark-red to brown (via dark green). The mixture was cooled to room temperature, and the excess of 1,2,4-triazole was removed by suspending the crude product in ethanol (5 mL) under ultrasound treatment and centrifugation. This operation was repeated three times. The separated complex was washed with ethanol and diethyl ether and dried at room temperature in air. Yield: 0.09 g, 40%. Anal. Calcd. for $C_8H_{12}N_{12}Cl_3Ru$ (M_r = 483.69 g/mol): C, 19.87; H, 2.50; N, 34.75; Cl, 21.99. Found: C, 19.85; H, 2.51; N, 34.58; Cl, 21.59. ESI-MS (positive): *m*/*z* 448 $[RuCl_2(Htrz)_4]^+$, 379 $[RuCl_2(Htrz)_3]^+$, 310 $[RuCl_2(Htrz)_2]^+$. IR spectrum in KBr, selected bands: 3118 s, 1523 vs, 1503 vs, 1416 vs, 1303 vs, 1153 vs, 1053 vs, 970 vs, 769 vs, br, 626 vs cm^{-1}. UV−vis (MeOH), λ_{max} (ϵ): 400 nm (2.77 mM^{-1} cm^{-1}). Solubility in water at 298 K: 18 mg/mL. Red-brown crystals of $[RuCl_2(Htrz)_4][SbF_6]·2H_2O$ (**C6a**·$2H_2O$) suitable for the X-ray diffraction study were obtained by a metathesis reaction of **C6** with Na[SbF_6] in water.

***trans*-[$Ru^{III}Cl_2$(Hpz)$_4$]Cl (C7).** A solution of (Hpz)[*trans*-$RuCl_4$(Hpz)$_2$] (**A7**) (4.00 g, 8.9 mmol) and pyrazole (1.20 g, 17.6 mmol) in ethanol/water (150 mL, 7:3) was refluxed for 7 h. The solution volume was reduced to ca. 10 mL, and the mixture was allowed to stand at 4 °C overnight. The wine-red needles formed were filtered off, washed with water (2 × 2 mL), and dried in a desiccator over P_4O_{10}. Yield: 3.60 g, 84%. Anal. Calcd for $C_{12}H_{16}N_8Cl_3Ru$ (M_r = 479.74 g/mol): C, 30.04; H, 3.36; N, 23.36; Cl, 22.17. Found: C, 30.29; H, 3.31; N, 23.05; Cl, 21.99. ESI-MS (positive): *m*/*z* 444 $[RuCl_2(Hpz)_4]^+$. IR spectrum in KBr, selected bands: 3127 s, 1471 s, 1113 vs, 1047 vs, 794 vs, 761 s, 601 s cm^{-1}. UV−vis (MeOH), λ_{max} (ϵ): 401 nm (3.71, mM^{-1} cm^{-1}). Solubility in water at 298 K: 6 mg/mL. Single crystals of **C7** suitable for the X-ray diffraction study were obtained from ethanol/water (7:3) at 4 °C.

***trans*-[$Ru^{II}Cl_2$(metrz)$_4$] (D4).** A mixture of *trans*-$[RuCl_2(MeCN)_4]$ (0.23 g, 0.68 mmol) and 1-methyl-1,2,4-triazole (0.5 mL) was heated at 130 °C for 1 h. The salmon solid was filtered off, washed with methanol and diethyl ether, and dried at room temperature in vacuo. Yield: 0.22 g, 64%. Anal. Calcd for $C_{12}H_{20}N_{12}Cl_2Ru$ (M_r = 504.34 g/mol): C, 28.58; H, 4.00; N, 33.33; Cl, 14.06. Found: C, 28.79; H, 3.79; N, 33.47; Cl, 13.82. ESI-MS (positive): *m*/*z* 504 $[RuCl_2(metrz)_4]^+$. IR spectrum in KBr, selected bands: 3141 s, 3125 s, 1535 vs, 1288 vs, 1214 vs, 1122 vs, 1112 vs, 1005 vs, 886 vs, 685 vs, 413 s cm^{-1}. ^1H NMR in DMSO-d_6: δ 8.76 [s, 4*H*, C(5)*H*], 8.24 [s, 4*H*, C(3)*H*], 3.89 [s, 12*H*, NCH_3].

[Ru^{II}(metrz)$_6$](SO_3CF_3)$_2$ (E4). A solution of $[Ru(DMF)_6](SO_3CF_3)_3$ (0.50 g, 0.51 mmol) and 1-methyl-1,2,4-triazole (0.5 mL) in anhydrous methanol (25 mL) was refluxed for 12 h. The white precipitate was filtered off, washed with methanol and diethyl ether, and dried in vacuo. Yield: 0.21 g, 46%. Anal. Calcd for $C_{20}H_{30}N_{18}F_6O_6RuS_2$ (M_r = 897.76 g/mol): C, 26.76; H, 3.37; N, 28.08, S, 7.14. Found: C, 26.56; H, 3.31; N, 27.73; S, 7.03. ESI-MS (positive): *m*/*z* 749 $[Ru(metrz)_6^{2+} + (SO_3CF_3)^-]^+$. ESI-MS (negative): *m*/*z* 149 $[SO_3CF_3]^-$. IR spectrum in KBr, selected bands: 3135 s, 1536 vs, 1265 vs, 1119 vs, 1033 vs, 1005 s, 683 s, 636 vs, 518 s, 409 s cm^{-1}. UV−vis (MeOH), λ_{max} (ϵ): 253 nm (12.20 mM^{-1} cm^{-1}). ^1H NMR in DMSO-d_6: δ 8.56 [s, 6*H*, C(5)*H*], 7.91 [s, 6*H*, C(3)*H*], 3.89 [s, 18*H*, NCH_3].

[Ru^{II}(metrz)$_6$](BF_4)$_2$ (E4b). A mixture of [Ru(1,5-cyclooctadiene)-$(MeCN)_4](BF_4)_2$ (0.17 g, 0.31 mmol) and 1-methyl-1,2,4-triazole (0.3 mL) was heated at 130 °C for 2 h. A white precipitate was deposited after the reaction mixture was cooled to room temperature. It was filtered off, washed with methanol and diethyl ether, and dried at room temperature in vacuo. Yield: 0.13 g, 54%. Colorless crystals suitable for the X-ray diffraction study were grown from MeOH/H_2O (8/2) at 4 °C. Anal. Calcd for $C_{18}H_{30}N_{18}B_2F_8Ru$ (M_r = 773.23 g/mol): C, 27.96; H, 3.91; N, 32.61. Found: C, 28.23; H, 3.65; N, 32.31. ESI-MS (positive): *m*/*z* 687 $[Ru(metrz)_6^{2+} + (BF_4)^-]^+$, 604 $[Ru(metrz)_5^{2+} + (BF_4)^-]^+$, 217 $[Ru(metrz)_4]^{2+}$. ESI-MS (negative): *m*/*z* 87 $[BF_4]^-$. IR spectrum in KBr, selected bands: 3155 s, 1536 vs, 1281 vs, 1119 s, 1050 vs, 1006 s, 686 vs, 521 m, 404 s cm^{-1}. UV−vis (MeOH), λ_{max} (ϵ): 252 nm (12.16 mM^{-1} cm^{-1}). ^1H NMR in DMSO-d_6: δ 8.56 [s, 6*H*, C(5)*H*], 7.91 [s, 6*H*, C(3)*H*], 3.89 [s, 18*H*, NCH_3].

[Ru^{II}(Htrz)$_6$][$ZnCl_4$] (E6c). $[Ru(MeCN)_6][ZnCl_4]·2.55H_2O$ (0.10 g, 0.17 mmol) was added to the molten 1*H*,2,4-triazole (0.50 g, 7.25 mmol), and the mixture was heated at 125 °C for 1 h. The molten mass was cooled to room temperature, and the excess of triazole was removed by dissolution in ethanol (4 mL) under ultrasound treatment and separated by centrifugation. This operation was repeated three times. The white-gray product was washed with ethanol, diethyl ether, and dried at room temperature in air. Yield: 0.05 g, 41 %. The compound is hardly soluble in any common solvent. Anal. Calcd. for $C_{12}H_{18}N_{18}Cl_4RuZn$ (M_r = 722.66 g/mol): C, 19.94; H, 2.51; N, 34.89. Found: C, 19.72; H, 2.73; N, 35.19. ESI-MS (positive): *m*/*z* 515 $[Ru(Htrz)_5(trz)]^+$, 377 $[Ru(Htrz)_3(trz)]^+$, 308 $[Ru(Htrz)_2(trz)]^+$. IR spectrum in KBr, selected bands: 3101 s, br, 1506 vs, 1430 s, 1162 vs, 1057 s, 1002 s, 632 vs cm^{-1}.

Results and Discussion

Synthesis of the Complexes. The synthetic routes to complexes **A**−**E** are summarized in Scheme 1. The **A** complexes were prepared starting from a hydrochloric acid solution of $RuCl_3$ and an excess of the azole ligand (L).[26]

Scheme 1. Synthetic Routes to Complexes **A**−**E**[a]

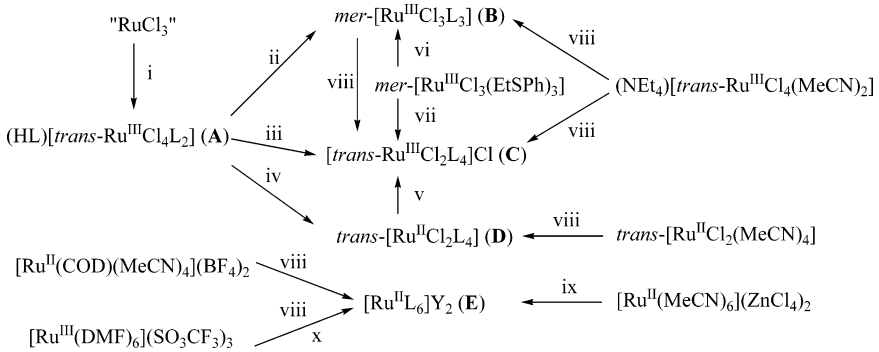

[a] (i) Aqueous hydrochloric acid/ethanol, reflux, L = Him, Hbeim, Hmepz, Htrz, Hpz, or Hind; (ii) ethanol/water (7:3) or THF, reflux, L = Hbeim, Hmepz, Hpz, or Hind; (iii) ethanol/water (7:3), reflux, L = Hbeim or Hpz; (iv) ethanol/water (7:3), reflux, L = Hind; (v) H_2O_2/HCl, MeOH, L = Hind; (vi) toluene, reflux, L = buim; (vii) toluene/ethanol, reflux, L = Him; (viii) 130 °C, L = metrz; (ix) 130 °C, L = Htrz; and (x) methanol, reflux, L = metrz.

The reaction of (HL)[*trans*-$Ru^{III}Cl_4L_2$] (**A**) with the azole ligand L in aqueous ethanol or THF yielded complexes *mer*-[$Ru^{III}Cl_3L_3$] (**B**) (L = Hbeim, Hmepz, Hpz, Hind[25]), *trans*-[$Ru^{III}Cl_2L_4$]Cl (**C**) (L = Hbeim, Hpz), and *trans*-[$Ru^{II}Cl_2(Hind)_4$].[9] The latter was oxidized with hydrogen peroxide in methanol in the presence of hydrochloric acid to form the Ru^{III} species.[9] Complexes **B1** and **C2** were prepared from [$Ru^{III}Cl_3(EtSPh)_3$] and an excess of azole ligand under reflux. **B6** can be converted into **C6** in molten 1,2,4-triazole at 130 °C. Complex **C6** can also be synthesized with a 30−32% yield starting from (Et_4N)[*trans*-$Ru^{III}Cl_4(MeCN)_2$] or $(DMSO)_2H$[*trans*-$Ru^{III}Cl_4(DMSO)_2$] (DMSO = S-bonded dimethyl sulfoxide) under similar experimental conditions by replacement of the *trans*-acetonitrile or dimethyl sulfoxide ligands, respectively, and the two chloro ligands by the 1,2,4-triazole. Complexes **B4** and **D4** were prepared from acetonitrile-based ruthenium complexes in the 1-methyl-1,2,4-triazole ligand at 130 °C. The **E** complexes resulted from the reaction of [Ru^{II}(1,5-cyclooctadiene)$(MeCN)_4$]$(BF_4)_2$, [$Ru^{II}(MeCN)_6$]$(ZnCl_4)_2$, and [$Ru^{III}(DMF)_6$]$(SO_3CF_3)_3$ with the molten azole ligand (L = Htrz, metrz) at 130 °C or with an excess of the azole ligand (L = metrz, Him[12]) in refluxing methanol.

Crystal Structures. The crystallographic data for complexes **B**, **C**, and **E** are given in Tables 1 and 2. All of the structures contain an essentially octahedral complex of the general formula *mer*-[$RuCl_3$(azole)$_3$], *trans*-[$RuCl_2$(azole)$_4$]$^+$, or [Ru(azole)$_6$]$^{2+}$. Tables S1−S9 with selected bond lengths and angles and other geometrical details of the complexes studied are given as Supporting Information.

The asymmetric unit of **B1** (Table S1) consists of two crystallographically independent molecules, **B1a** (Figure 2) and **B1b** (Figure S1) with comparable metric parameters. The differences observed between the metal−ligand bond lengths in **B1a** [Ru−N, av. 2.0759(76) Å[27] and Ru−Cl, av. 2.3634(31) Å] and **B1b** [Ru−N, av. 2.0726(28) and Ru−Cl, av. 2.3640(83) Å] are quite small. In contrast, the positions of the imidazole rings around ruthenium are markedly different (see Supporting Information); this is probably the result of the lack of intra- and intermolecular hydrogen bonding interactions in the crystal structure of **B1**.

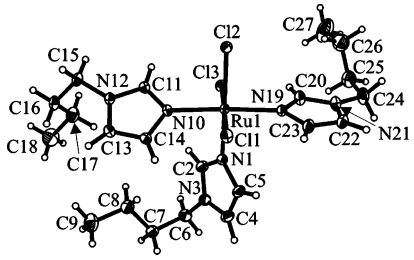

Figure 2. ORTEP view of the first independent molecule of [$Ru^{III}Cl_3$-(buim)$_3$] (**B1a**), showing the atom-numbering scheme. Thermal displacement ellipsoids are drawn at the 50% probability level.

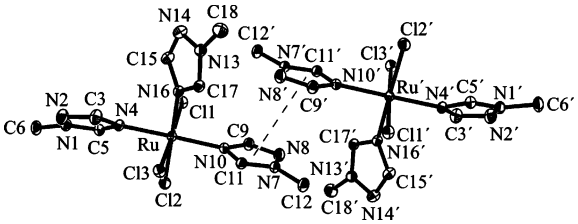

Figure 3. Part of the crystal structure of [$Ru^{III}Cl_3$(metrz)$_3$] (**B4**) showing the formation of a stack pair by $\pi-\pi$ interactions between two adjacent metrz ligands. H atoms are omitted for clarity. Displacement ellipsoids are drawn at the 50% probability level.

Coordination of metrz ligands to ruthenium(III) in **B4** (Figure 3, Table S2) occurs via N4 of 1-methyl-1,2,4-triazole. The Ru−N bond distances [av. 2.0768(51) Å] are comparable with those in [$RuCl_3$(1,3-thiazole)$_3$],[28] and the Ru−Cl bond distances [av. 2.3521(68) Å] do not present unexpected features.[2,29] The orientation of the triazole ligands appears to be stabilized by intermolecular interactions of the type C−H···Cl and $\pi-\pi$ intermolecular interactions between the triazole planes (Figure 3). For the interacting triazole rings of the adjacent molecules, the minimum distance between the ring centroids is ∼3.7 Å, with the planes separated by ∼3.5 Å.

Complex **B5** (Figure 4, Table S3) crystallized in the orthorhombic noncentrosymmetric space group $P2_12_12_1$. The two Ru−N bonds, trans to each other [av. 2.0540(36) Å],

(27) For a sample of n observations x_i, the unweighted mean value (x_u) with its standard deviation (σ) was calculated using the following equations: $x_u = \sum_i x_i/n$ and $\sigma = \{\sum_i(x_i - x_u)^2/[n(n-1)]\}^{1/2}$.

(28) Pifferi, C.; Cini, R. *Acta Crystallogr.* **2000**, *C56*, e439−e440.
(29) Ziegler, M.; Monney, V.; Stoeckli-Evans, H.; Von Zelewsky, A.; Sasaki, I.; Dupic, G.; Daran, J.-C.; Balavoine, G. G. A. *J. Chem. Soc., Dalton Trans.* **1999**, 667−675.

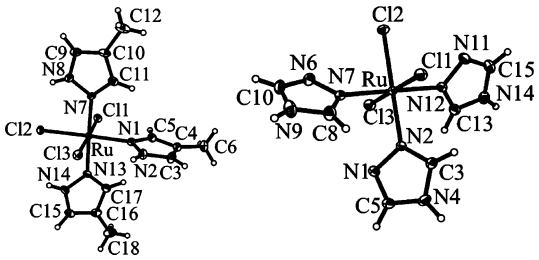

Figure 4. Molecular structures of $[Ru^{III}Cl_3(Hmepz)_3]$ (**B5**, left) and $[Ru^{III}Cl_3(Htrz)_3]$ (**B6**, right) in **B6**·H_2O showing the atom-numbering schemes. Thermal displacement ellipsoids are drawn at the 50% probability level.

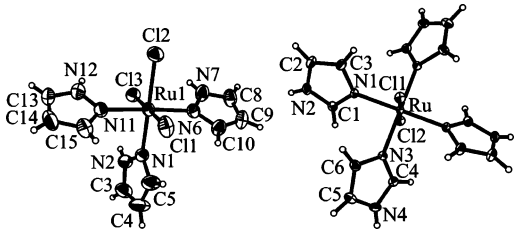

Figure 5. ORTEP view of the first independent molecule of $[Ru^{III}Cl_3(Hpz)_3]$ (**B7a**, left) and the $[Ru^{III}Cl_2(Him)_4]^+$ cation (right) in **C2**, showing the atom-numbering scheme. Thermal displacement ellipsoids are drawn at the 50% probability level.

are markedly shorter than the Ru−N1 bond [2.0793(17) Å] which is trans to Ru−Cl2. The difference in the Ru−Cl bonds is even more significant. The Ru−Cl2 bond length at 2.3912(6) Å is ∼55 σ longer than Ru−Cl1 and Ru−Cl3 at 2.3468(6) and 2.3413(6) Å, respectively. The largest deviations of the bond angles at the ruthenium atom from 90 and 180° do not exceed 2°.

In **B6**·H_2O (Figure 4, Table S4), the triazole ligands, which adopt the 4*H*-tautomeric form, are coordinated to ruthenium through N2 in the nomenclature used for 1*H*- or 4*H*-1,2,4-triazole. The Ru−N bond distances [av. 2.0721(29) Å] are only marginally shorter than those in **B4** [av. Ru−N 2.0768(51) Å], where the triazole ligands are bonded to the Ru atom via N4 (Table S2). The Ru−Cl bond distances have the same values within 3.8 σ and are in the range of 2.3427(8)−2.3469(6) Å, very close to the Ru^{III}−Cl bond lengths for $[RuCl_3(1,3\text{-thiazole-}N)_3]$.[28]

As for **B1**, the asymmetric unit of **B7** (Table S5) consists of two independent molecules with comparable geometries. Only small differences are observed in the metal−ligand bond distances in **B7a** [Figure 5; Ru−N, av. 2.0619(59) Å; Ru−Cl, av. 2.3638(70) Å] and **B7b** (Figure S2; Ru-N, av. 2.0645(10) Å; Ru−Cl, av. 2.3632(94) Å]. Each of the two independent molecules forms an infinite chain along the *b* axis; the chains are parallel to each other and are stabilized by stacking $\pi-\pi$ interactions between the trans-coordinated pyrazole ligands of adjacent molecules (Figure S3). For the interacting pyrazole rings, the minimum distance between the ring centroids is 3.56 Å for the first independent molecule and 3.63 Å for the second. Additional weak interactions of the C−H···Cl type are observed in the chain formed by **B7b**.

The crystal structure of **C2** (Figure 5, Table S6) consists of $[RuCl_2(Him)_4]^+$ cations and Cl^- anions, which form sheets parallel to the *ac* cell plane through N−H···Cl hydrogen bonding interactions. Each chloride ion forms four hydrogen

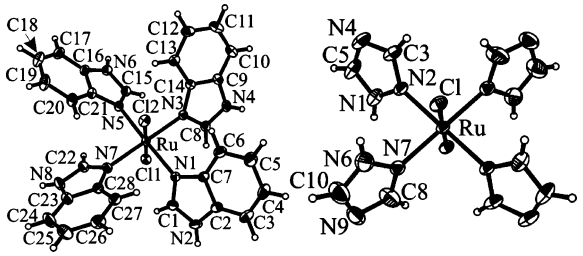

Figure 6. Structures of the $[Ru^{III}Cl_2(Hbeim)_4]^+$ cation (left) in **C3**·CH_3OH·$(C_2H_5)_2O$ and the $[Ru^{III}Cl_2(Htrz)_4]^+$ cation (right) in **C6a**·$2H_2O$ showing the atom-numbering schemes. Thermal displacement ellipsoids are drawn at the 50% probability level.

bonds with four imidazole rings of four neighboring cations (Figure S4). The Ru atom and the chloro ligands, Cl1 and Cl2, lie on a 2-fold rotation axis. The Ru−N1 and Ru−N3 bond lengths are 2.0687(12) and 2.0682(12) Å, respectively, and the Ru−Cl1 and Ru−Cl2 bond lengths are 2.3379(6) and 2.3458(6) Å, respectively. The bond angles at the Ru atom deviate from 90 and 180° by not more than 0.9°.

The crystal structure of **C3**·CH_3OH·$(C_2H_5)_2O$ (Figure 6, Table S7) consists of the complex cation $[RuCl_2(Hbeim)_4]^+$, a chloride counteranion, a molecule of methanol, and a molecule of diethyl ether. The Ru−N bond lengths [av. 2.0771(36) Å] are, on average, slightly longer than those in the imidazole complex **C2**, and the Ru−Cl1 and Ru−Cl2 bond lengths at 2.3570(8) and 2.3232(8) Å, respectively, are comparable to those in $[Ru^{III}Cl_2(Hind)_4]Cl\cdot 2CH_3OH$.[9] The maximal deviation of bond angles at Ru from 90 and 180° does not exceed 3°. Multiple hydrogen bonds are formed between the complex cations, the counteranion, and the solvent molecules in **C3**·CH_3OH·$(C_2H_5)_2O$ (Figure S5).

The ruthenium and antimony atoms of *trans*-$[Ru^{III}Cl_2(Htrz)_4][SbF_6]\cdot 2H_2O$ (**C6a**·$2H_2O$, Figure 6, Table S8) lie on crystallographic inversion centers, and the four triazole ligands are bonded to ruthenium via N2. The Ru−N [av. 2.0735(5) Å] and the Ru−Cl1 [2.3289(10) Å] bond lengths are comparable to those in **B6**. The Ru^{III}−Cl bond distance is markedly shorter than the Ru^{II}−Cl bond lengths in $[Ru^{II}Cl_2(4\text{-methylpyrimidine})_4]$ at 2.398(4) and 2.400(4) Å.[30] The cations are arranged in parallel chains, which are stabilized by strong intrachain hydrogen bonding interactions, N6−H6···N4′ ($-x+2$, $-y-1$, $-z-1$) with N6−H6 0.860, H6···N4′ 2.092, and N6···N4′ 2.901 Å and ∠N6−H6···N4′ 156.48° (Figure S6), and the water molecules are involved in the intermolecular hydrogen bonding interactions. Bond lengths and angles in the $[SbF_6]^-$ anion are similar to those reported elsewhere.[31]

The asymmetric unit of **C7** (Figure 7, Table S9) consists of two independent halves of the complex cations with ruthenium atoms Ru1 and Ru2 located on the crystallographic inversion centers and one chloride anion. The Ru−N bond lengths [av. 2.0603(24) Å] are shorter than those in $[RuCl_2(Hind)_4]^+$ at 2.069(5) and 2.071(3) Å.[9] The Ru1−Cl1 and Ru2−Cl2 bond lengths at 2.3767(9) and 2.3565(7) Å,

(30) Bellucci, C.; Cini, R. *Acta Crystallogr.* **2001**, *C57*, 1039−1040.
(31) Cadierno, V.; Díez, J.; García-Álvarez, J.; Gimeno, J. *Chem. Commun.* **2004**, 1820−1821.

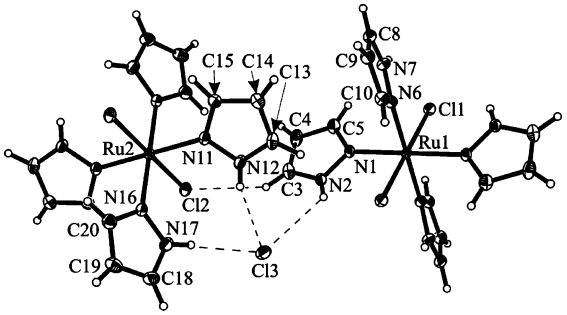

Figure 7. Perspective view of a part of the crystal structure of $[Ru^{III}Cl_2(Hpz)_4]Cl$ (**C7**).

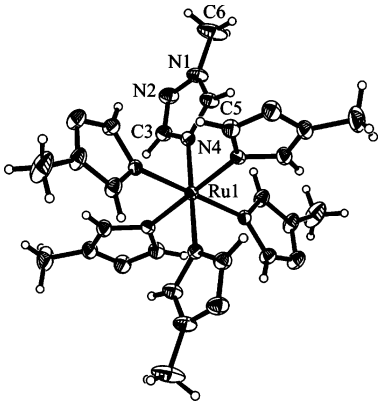

Figure 8. ORTEP view of $[Ru(metrz)_6]^{2+}$ in **E4b** with 50% probability of thermal ellipsoids.

respectively, are, in contrast, longer than those in the indazole complex at 2.3285(9) and 2.3338(9) Å, respectively.

Complex **E4b** (Figure 8) crystallizes in the trigonal space group $R\bar{3}$ with a Ru atom at a point of S_6 symmetry and Ru−N bond lengths of 2.093(2) Å. The same or very similar bond distances have been documented for the homoleptic six-coordinate ruthenium(II) complexes of imidazole derivatives (e.g., $[Ru(5Hmeim)_6](CF_3SO_3)_2$ at 2.093(2) Å $[Ru(1meim)_6](CF_3SO_3)_2$ at 2.100(2) Å,[32] $[Ru(Him)_6]CO_3\cdot 5H_2O$ at 2.102(2) Å,[33] and $[Ru(1meim)_6]Cl_2\cdot 2H_2O$ with the three independent Ru−N distances averaging 2.106(8) Å).[34] The cis N−Ru−N angles are essentially orthogonal.

Electrochemical Studies. Ru^{III}/Ru^{II} Redox Process. The cyclic voltammograms (CVs) of complexes **A**, **B**, and **C** in DMF or DMSO electrolyte solution display (Figures 9 and 10) one single-electron $Ru^{III} \rightarrow Ru^{II}$ reduction wave, I^{red}. The reactions induced by electron transfer at I^{red} are discussed below. In the case of **D** and **E**, the observed reversible single-electron oxidation wave, I^{ox}, is caused by the $Ru^{II} \rightarrow Ru^{III}$ process. The redox potential values for the Ru^{III}/Ru^{II} redox couple (wave I) are in the ranges of −0.74 to −0.41 (**A**), −0.50 to 0.10 (**B**), −0.18 to 0.59 (**C** and **D**), and 0.50 to 1.04 (**E**) V vs NHE (Tables 3 and 4) following the order expected, resulting from the effects of the complex charge and the number of strong electron-donor chloro ligands.

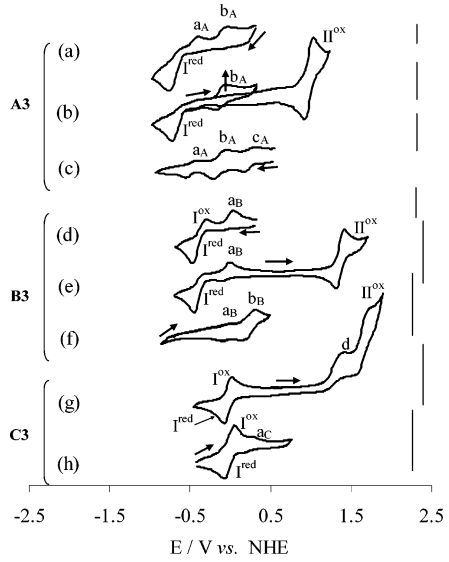

Figure 9. Cyclic voltammograms of 1.5 mM solutions in DMF with 0.15 M $[n\text{-}Bu_4N][BF_4]$ of $(H_2beim)[trans\text{-}RuCl_4(Hbeim)_2]$, **A3** (a−c), *mer*-$[RuCl_3(Hbeim)_3]$, **B3** (d−f), *trans*-$[RuCl_2(Hbeim)_4]Cl$, **C3** (g and h) at a glassy carbon electrode (a−c) or at a platinum working electrode (d−h) at a scan rate of 0.70 V s^{-1} (a and d) or 0.20 V s^{-1} (b, e, and g). The CVs of c, f, and h were recorded after exhaustive cathodic CPE at the reduction wave I^{red} at 0.20 V s^{-1}. The solid line on the right refers to the current (1 μA). For the assignment of the waves, see text.

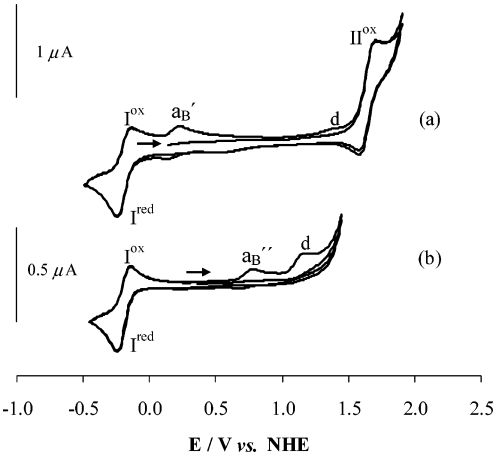

Figure 10. Cyclic voltammograms of 1.5 mM *mer*-$[RuCl_3(metrz)_3]$ (**B4**) solutions in DMF (a) or DMSO (b) with 0.15 M $[n\text{-}Bu_4N][BF_4]$, at a platinum working electrode and at a scan rate of 0.05 V s^{-1}. Wave a_B' or a_B'' is assigned to the Ru^{II}/Ru^{III} redox couple of $[RuCl_2(metrz)_3(DMF)]$ or $[RuCl_2(metrz)_3(DMSO)]$, respectively. Wave d is the result of the oxidation of the cathodically liberated Cl^- ligand, and wave II^{ox} corresponds to the Ru^{III}/Ru^{IV} redox couple.

The Ru^{III}/Ru^{II} redox potential values of complexes containing ligands Him, Htrz, Hpz, and Hind agree (Table 3, 4) with the predicted ones from eq 1 proposed by Lever,[35] using the known values of S_M and I_M for that redox couple (0.97 and 0.04 V vs NHE, respectively)[35] and the known E_L values for the various ligands [$E_L(Cl^-) = -0.24$,[35] $E_L(Him) = 0.09$,[34] $E_L(Htrz) = 0.18$,[35] $E_L(Hpz) = 0.20$,[35] and $E_L(Hind) = 0.26$ V vs NHE,[6] Table 5]. In addition, the application of eq 1 allowed the estimate of the yet unknown E_L ligand parameters for buim (**1**, $E_L = 0.06$ V), Hbeim

(32) Baird, I. R.; Rettig, S. J.; James, B. R.; Skov, K. A. *Can. J. Chem.* **1998**, *76*, 1379−1388.
(33) Anderson, C.; Beauchamp, A. L. *Inorg. Chem.* **1995**, *34*, 6065−6073.
(34) Clarke, M. J.; Bailey, V. M.; Doan, P. E.; Hiller, C. D.; LaChance-Galang, K. J.; Daghlian, H.; Mandal, S.; Bastos, C. M.; Lang, D. *Inorg. Chem.* **1996**, *35*, 4896−4903.
(35) (a) Lever, A. B. P. *Inorg. Chem.* **1990**, *29*, 1271−1285. (b) Lever, A. B. P.; Dodsworth, E. S. *Inorganic Electronic Structure and Spectroscopy*; Wiley: New York, 1999; pp 227−290.

Table 3. Cyclic Voltammetric Data for Complexes **A**−**C** and Their Corresponding Estimated Redox Potentials

com-plexes	$E_{1/2}$/I^{red}		$E_{1/2}$/a[c]		$E_{1/2}$/b[c]		$E_{1/2}$/II^{ox}	
	exptl[a]	calcd[b]	exptl[a]	calcd[b]	exptl[a]	calcd[b]	exptl[a]	calcd[b]
A2[e]	−0.72*	−0.72	−0.49	−0.45	−0.15	−0.19	0.96	0.88
	(−0.74)*						(0.99)	
A3	−0.68*	−	−0.43	−	−0.12	−	0.98	−
	(−0.65)*						(1.05)	
A6[e]	−0.48*	−0.54	−0.21	−0.28	0.03	−0.02	1.18	1.06
	(−0.44)*						(1.19)	
A8[e]	−0.43*	−0.39	−0.15	−0.12	0.16	0.14	1.27	1.23
	(−0.41)*						(1.27)	
B1	−0.50	−	−0.13	−	0.15[d]	−	1.33	−
	(−0.46)		(0.48)				(1.32)	
B3	−0.41	−	−0.06	−	0.24[d]	−	1.35	−
	(−0.38)		(0.53)				(1.33)	
B4	−0.18	−	0.14	−	0.41[d]	−	1.61	−
	(−0.20)		(0.92)				−	
B5	−0.13	−	0.19	−	0.44[d]	−	1.46*	−
	(−0.13)		(0.74)				(1.43)*	
B6·H_2O	−0.07	−0.13	0.19	0.13	0.36[d]	0.39	1.43	1.49
	(−0.09)		(0.60)	(0.65)		(1.44)	(1.39)	
B7	−0.10	−0.08	0.21	0.19	0.38[d]	0.45	1.53	1.56
	(−0.11)		(0.74)	(0.71)		(1.50)	−	
B8	0.10	0.10	0.38	0.36	−	0.62	−	1.74
	(0.09)		(0.93)[d]	(0.88)		(1.67)		
C2	−0.15	−0.08	0.05[d]	0.19	−	0.45	1.70	1.56
	(−0.18)		(0.47)[d]	(0.71)		(1.50)	−	
C3	−0.03	−	0.24[d]	−	−	−	1.63	−
	(−0.03)		(0.92)[d]				−	
C6	0.24	0.27	−	0.53	−	0.80	−	1.93
	(0.20)			(1.06)		(1.84)		
C7	0.35	0.35	−	0.61	−	0.87	−	2.01
	(0.30)			(1.14)		(1.92)		
C8	0.59	0.58	−	0.85	−	1.11	−	2.26
	(0.56)			(1.37)		(2.15)		

[a] Experimental redox potentials in V ± 0.02 vs NHE in 0.15 M [*n*-Bu_4N][BF_4]/DMF (or DMSO, in parentheses). $E_{1/2}$ values are given for the reversible waves, whereas for the irreversible ones, the $E_{p/2}$ values are labelled with an asterisk. [b] Redox potentials in V vs NHE estimated from eq 1 with S_M and I_M values of 0.97 and 0.04 V, respectively, and known E_L values for the ligands (see text). Values in brackets refer to the DMSO derivatives. [c] Oxidation waves detected upon scan reversal after the reduction process (wave I^{red}, see text). [d] Redox potentials for waves observed only on a CV scan after CPE. [e] Ref 6.

Table 4. Cyclic Voltammetric Data for Complexes **D** and **E** and Their Corresponding Estimated Redox Potentials

complexes	$E_{1/2}$/I^{ox}	
	exptl[a]	calcd[b]
D4	0.26	−
	(0.24)	
D8	0.58	0.58
	(0.56)	
E2	0.56	0.56
	(0.50)	
E4	1.04	−
	(1.00)	

[a] Experimental redox potentials in V ± 0.02 vs NHE in 0.15 M [*n*-Bu_4N][BF_4]/DMF (or DMSO, in parentheses). [b] Predicted redox potentials in V vs NHE as estimated from eq 1 with S_M and I_M values of 0.97 and 0.04 V, respectively, and known E_L values for the ligands (see text).

(**3**, E_L = 0.10 V), metrz (**4**, E_L = 0.17 V), and Hmepz (**5**, E_L = 0.18 V, Table 5).

$$E_{1/2}^{\text{pred}}\,(\text{V}) = S_M \sum E_L + I_M \qquad (1)$$

A linear dependence (eq 2) is found when plotting the E_L parameters of azole ligands **1**−**8** against the pK_a values of the corresponding azolium ions (Table 5, Figure 11). This gives a convenient method of obtaining a good estimate of the relatively rare (compared to the large amount of known pK_a values[36]) E_L parameters for azole ligands.

Table 5. Ligand Electrochemical Parameters (E_L Values in V vs NHE) and Basicities (pK_a Values for the Free Azolium Acids H_2L^+) for Ligands **1**−**8**

ligand	E_L	pK_a
buim (**1**)	0.06[a]	7.16[e]
Him (**2**)	0.09[b]	6.65[f]
Hbeim (**3**)	0.10[a]	5.63[g]
metrz (**4**)	0.17[a]	3.20[e]
Hmepz (**5**)	0.18[a]	3.25[h]
Htrz (**6**)	0.18[c]	2.55[i]
Hpz (**7**)	0.20[c]	2.64[j]
Hind (**8**)	0.26[d]	1.25[j]

[a] Values estimated from eq 1 using the known[35] values of S_M, I_M, and E_L for the other ligands (see text). [b] Ref 34. [c] Ref 35. [d] Ref 6. [e] Ref 36. [f] Albert, A. *Physical Methods in Hetrocyclic Chemistry*, Vol. I; Katritzky, A. R., Ed.; Academic Press, New York, 1963. [g] Kapinos, L. E.; Song, B.; Sigel, H. *Chem.*−*Eur. J.* **1999**, *5*, 1794−1802. [h] Boraei, A. A. A. *Spectrochim. Acta* **2002**, *A58*, 1895−1901. [i] Potts, K. T. *Chem. Rev.* **1961**, *61*, 87−127. [j] Catalán, J.; Claramunt, R. M.; Elguero, J.; Laynez, J.; Menéndez, M.; Anvia, F.; Quian, J. H.; Taagepera, M.; Taft, R. W. *J. Am. Chem. Soc.* **1988**, *110*, 4105−4111.

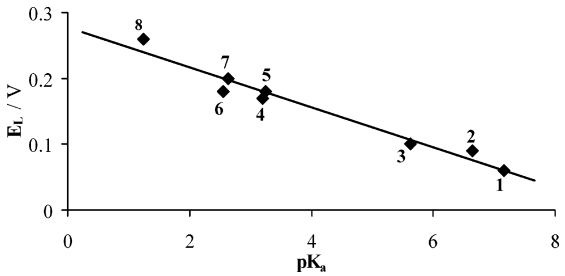

Figure 11. Plot of the E_L parameters of azole ligands **1**−**8** against the pK_a values of the corresponding azolium ions (Table 5): E_L (V) = 0.277 − 0.0302pK_a (r = 0.98).

$$E_L\,(\text{V}) = 0.277 - 0.0302\text{p}K_a \quad (r = 0.98) \qquad (2)$$

The electronic absorption spectra of Ru^{III} complexes **B** and **C** in methanol show one main band with an absorption maximum in the 347−381 and 346−452 nm ranges (Table S10), respectively, attributable to the azole or chloro ligand p$\pi \rightarrow$ Ru t_{2g} LMCT transition. As for the **A** complexes (in water),[6] the LMCT band for **B** and **C** (in MeOH) is blue shifted with increasing basicity and electron donor properties of the ligands. As expected,[35b] the Ru^{III}/Ru^{II} redox potential (Table 3) correlates (Figure 12, S7) with its transition energy for complexes **B** (eq 3) and **C** (eq 4). A negative slope is observed for both series of complexes because an increase of the metal-centered Ru^{III}/Ru^{II} redox potential results in a shift to lower energy for the LMCT transition.

$$h\nu\,(\text{eV}) = -0.523E_{1/2}[\text{Ru}^{III/II}] + 3.273 \quad (r = 0.97) \quad (\text{for } \mathbf{B}) \qquad (3)$$

$$h\nu\,(\text{eV}) = -1.087E_{1/2}[\text{Ru}^{III/II}] + 3.400 \quad (r = 0.99) \quad (\text{for } \mathbf{C}) \qquad (4)$$

(36) Catalán, J.; Abboud, J. L. M.; Elguero, J. *Adv. Heterocycl. Chem.* **1987**, *41*, 187−274 and references therein.

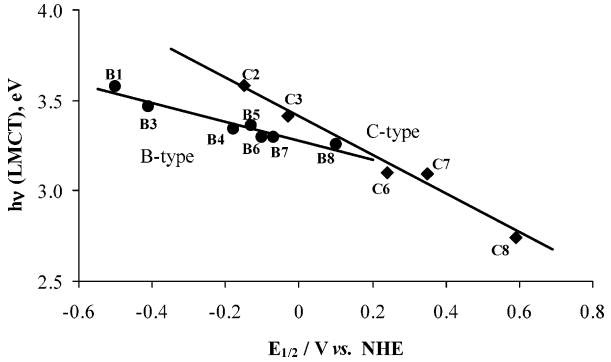

Figure 12. Plot of the LMCT transition energy against $E_{1/2}$ (Ru^{III}/Ru^{II}) for complexes **B** (●) and **C** (◆). The electrochemical data are shown in Table 3, and the optical data are in Table S10: $h\nu$ (eV) = $-0.523E_{1/2}[Ru^{III/II}] + 3.273$ ($r = 0.97$) (for **B**) and $h\nu$ (eV) = $-1.087E_{1/2}[Ru^{III/II}] + 3.400$ ($r = 0.99$) (for **C**); λ (nm) = $55.9E_{1/2}[Ru^{III/II}] + 378.6$ ($r = 0.97$) (for **B**) and λ (nm) = $136.1E_{1/2}[Ru^{III/II}] + 365.2$ ($r = 0.99$) (for **C**).

Ru^{III}/Ru^{IV} Redox Process. Complexes **A**, **B** (except **B8**), **C2**, and **C3**, studied by CV under the above experimental conditions, show one reversible (irreversible only in the case of **B5**) single-electron $Ru^{III} \rightarrow Ru^{IV}$ oxidation wave (wave II^{ox}, Figures 9b, e, and g and 10a) at potential values of 0.96−1.27 (**A**), 1.32−1.61 (**B**), and 1.63−1.70 (**C2**, **C3**) V vs NHE in DMF or DMSO (Table 3). The redox potentials agree satisfactorily with those predicted by Lever's equation, applying the above-mentioned E_L parameters (Table 5) and the reported S_M and I_M values for the Ru^{III}/Ru^{IV} redox couple (1.03 and 1.68 V, respectively)[6] (Table 3). For the **C** complexes, the oxidation of the chloride counterion is detected (wave *d*, Figure 9g) at $E_p = 1.20-1.35$ V vs NHE.

Solvolysis Upon Ru^{III} Reduction. Cathodically induced metal dechlorination on solvolysis is common[37] and has already been documented in detail for the **A** complexes.[6] Thus, the replacement of the first chloro ligand by solvent S upon reduction of *trans*-$[RuCl_4L_2]^-$ (**A**) at I^{red} results in the formation of the monosolvento product $[Ru^{II}Cl_3L_2S]^-$, which is oxidized (wave a_A, Figure 9a) at −0.49 to −0.15 V; $[Ru^{II}Cl_2L_2S_2]$ is detected (wave b_A, Figure 9b) at a sufficiently low scan rate in DMF at −0.15−0.16 V, and a CV scan after the cathodic CPE at wave I^{red} reveals the formation of the trisolvento species $[Ru^{II}ClL_2S_3]^+$ (wave c_A, Figure 9c) at 0.22−0.43 V vs NHE in DMF.

For the **B** complexes, $[Ru^{II}Cl_2L_3S]$ (wave a_B) is detected by CV upon scan-reversal following the reduction of $Ru^{III} \rightarrow Ru^{II}$ at −0.13−0.38 V in DMF (Figures 9d and e and 10a) and 0.48−0.74 V in DMSO (Figure 10b, Scheme 2). Formation of the disolvento complex $[RuClL_3S_2]^+$ (wave b_B, Figure 9f) is only observed by CV upon CPE at I^{red} at 0.15−0.44 V. CVs of the **C** complexes do not reveal any species formed upon reduction (Figure 9g), but CVs after the cathodic CPE of I^{red} in **C2** and **C3** show the formation, to some extent, of $[RuClL_4S]^+$ (wave a_C, Figure 9h, Table 3).

Scheme 2. Proposed Anodic and Cathodic Processes for the **B** Complexes (S = DMF or DMSO).

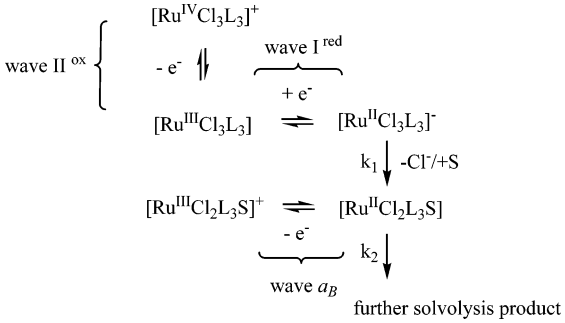

Complexes **C6**−**C8** (upon reduction to Ru^{II}) and the ruthenium(II) **D** complexes remained unchanged in the electrolyte solution, and no solvolysis products were observed within several hours.

The formation of waves a, b, or c upon reduction at I^{red} is accompanied by the liberation of chloride, which is detected by its irreversible oxidation wave (wave d) at $E_p = 1.20-1.35$ V (Figure 10), consistent with reported observations.[2,6,38] The redox potentials of the solvento complexes are in good accord with those predicted by Lever's equation [E_L(DMSO) = 0.57,[39a] and E_L(DMF) = 0.03,[39b] Table 3]. The accelerated solvolysis upon reduction for the **A** complexes compared to those of **B** and **C** is in agreement with qualitative observations for the reduction-induced halide substitution of the $[RuCl_{6-n}(RCN)_n]^z$ complexes, where the rate of chloro ligand replacement upon electrochemical reduction decreases with an increasing number of nitrile ligands, *n*, in the complex (which is concomitant with an increase of the Ru^{III}/Ru^{II} redox potential).[37c]

Kinetic Studies. The mechanism proposed in Scheme 2 was investigated by digital simulation (ESP program).[40] A good fit was obtained for the degree of reversibility of the cathodic wave I^{red} (i.e., ${}^{I}i_p^{ox}/{}^{I}i_p^{red}$) and the extent of the formation of the chloro ligand displacement product (i.e., the normalized peak−current of wave a, $\rho = {}^{a}i_p^{ox}/{}^{I}i_p^{red}$) as a function of scan rate for the **B** complexes (Table 6, Figure 13). No significant variation of the above behavior was detected upon changing the concentration of the complexes, thus indicating the involvement of first-order chemical steps.

The optimized values of the homogeneous rate constants k_1 and k_2 (Table 6) for the first and second, respectively, replacement of the chloro ligands by DMF or DMSO upon reduction generally increase with a decrease of the redox potential of the corresponding complex as expressed by a decrease of their $\sum E_L$ values. The overall chloro ligand labilization toward displacement by the solvent is thus promoted by an increase of the electron donor minus acceptor ability of the coligands. The plot of the homogeneous rate constants k_1 and k_2 (logarithmic scale) of the **B** complexes,

(37) (a) Salih, T. A.; Duarte, M. T.; Fraústo da Silva, J. J. R.; Galvão, A. M.; Guedes da Silva, M. F. C.; Hitchcock, P. B.; Hughes, D. L.; Pickett, C. J.; Pombeiro, A. J. L.; Richards, R. L. *J. Chem. Soc., Dalton Trans.* **1993**, 3015−3023. (b) Costa, G.; Balducci, G.; Alessio, E.; Tavagnacco, C.; Mestroni, G. *J. Electroanal. Chem.* **1990**, *296*, 57−76. (c) Duff, C. M.; Heath, G. A. *J. Chem. Soc., Dalton Trans.* **1991**, 2401−2411.

(38) Serli, B.; Zangrando, E.; Iengo, E.; Mestroni, G.; Yellowlees, L.; Alessio, E. *Inorg. Chem.* **2002**, *41*, 4033−4043.

(39) (a) Guedes da Silva, M. F. C.; Pombeiro, A. J. L.; Geremia, S.; Zangrando, E.; Calligaris, M.; Zinchenko, A. V.; Kukushkin, V. Yu. *J. Chem. Soc., Dalton Trans.* **2000**, 1363−1371. (b) http://www.chem.yorku.ca/profs/lever (homepage of A. B. P. Lever).

(40) Nervi, C.; *Electrochemical Simulation Package*, version 2.4; Dipartimento di Chimica IFM: Torino, Italy, 1994/98, nervi@lem.ch.unito.it.

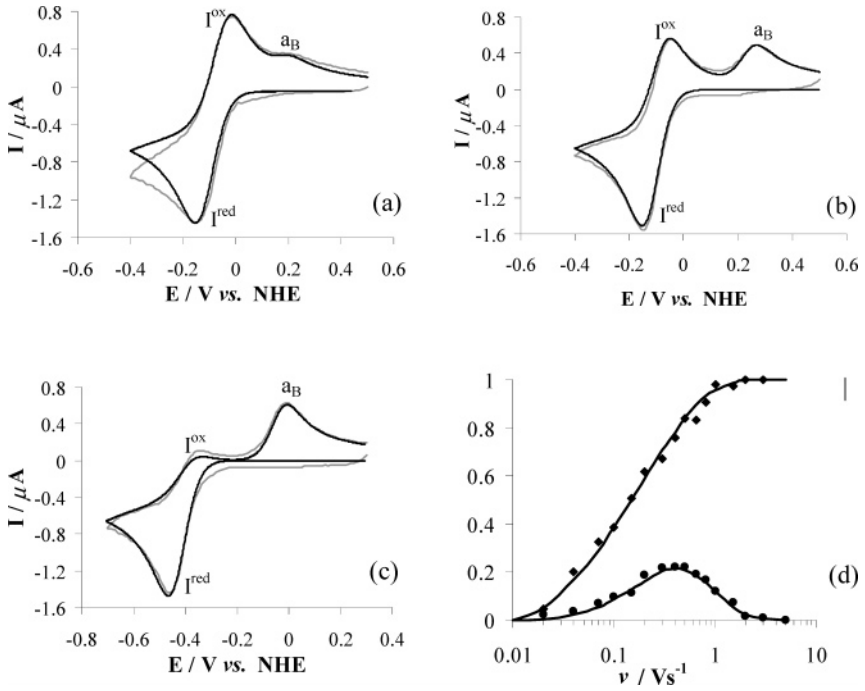

Figure 13. Experimental (1.5 mM, gray line) and simulated cyclic voltammograms (black line) for *mer*-$[RuCl_3(Htrz)_3]\cdot H_2O$ (**B6**·H_2O) (a), *mer*-$[RuCl_3(Hpz)_3]$ (**B7**) (b), and *mer*-$[RuCl_3(Hbeim)_3]$ (**B3**) (c) in DMF with 0.15 M $[n\text{-}Bu_4N][BF_4]$ at a platinum disk working electrode and at a scan rate of 0.30 V s^{-1}. Figure 11d provides experimental (symbols) and theoretical (solid lines) variations of the reversibility of the Ru^{III}/Ru^{II} reduction wave I^{red}, ${}^{I}i_p^{ox}/i_p^{red}$ (◆), and of the parameter $\rho = {}^{a}i_p^{ox}/{}^{I}i_p^{red}$ (●) as a function of scan rate (logarithmic scale) for compound *mer*-$[RuCl_3(Hpz)_3]$ (**B7**). The experimental error bar is shown at the top right corner. The simulated voltammograms (a−c) and theoretical lines in (d) were obtained by using the optimized values of the rate constants given in Table 6.

Table 6. Kinetic Rate Constants,[a] k_1 and k_2, for the Cl^- Replacement by DMF (or DMSO, in parentheses) for the **B** Compounds

compound	k_1 (s^{-1})	k_2 (s^{-1})
B1	20 ± 3	0.5 ± 0.3
	(19 ± 3)	(<0.03)
B3	4.0 ± 0.7	0.1 ± 0.05
	(3.5 ± 0.5)	(<0.03)
B4	0.18 ± 0.03	0.05 ± 0.03
	(0.13 ± 0.03)	(<0.03)
B5	0.8 ± 0.1	0.03 ± 0.02
	(0.7 ± 0.2)	(<0.03)
B6	0.15 ± 0.03	0.06 ± 0.03
	(0.12 ± 0.03)	(<0.03)
B7	0.60 ± 0.05	0.05 ± 0.03
	(0.6 ± 0.1)	(<0.03)
B8	0.07 ± 0.02	< 0.03
	(<0.1)	−

[a] The homogeneous rate constants k_1 and k_2 (in s^{-1} ± estimated confidence interval) were determined by using the ESP simulation program (ref 40) with k_{het} between 5×10^{-2} and 5×10^{-3} cm s^{-1}.

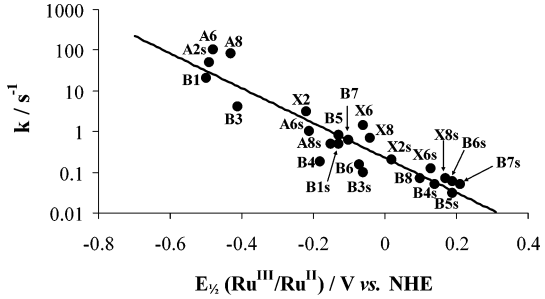

Figure 14. Plot of the kinetic rate constants k_1 and k_2 (first and second replacement, respectively, of chloro ligands by DMF upon reduction) in s^{-1} (logarithmic scale) against the redox potential of the Ru^{III}/Ru^{II} process in V vs NHE for the following complexes: $(H_2im)[trans\text{-}RuCl_4(Him)(DMSO)]$ (**X2**), $(H_2trz)[trans\text{-}RuCl_4(Htrz)(DMSO)]$ (**X6**), $(H_2ind)[trans\text{-}RuCl_4(Hind)(DMSO)]$ (**X8**), **A2** (only k_2), **A6**, **A8**,[6] **B1**, **B3**−**B8**, and their solvolyzed species (with index **s**) in DMF (replacement of one chloro ligand by one DMF ligand). $\log k\ (s^{-1}) = -4.280E_{1/2}\ (V) - 0.647$ ($r = 0.93$).

the recently[6] reported ones of the **A** complexes, and those of (HL)[*trans*-$RuCl_4L(DMSO)$] (**X**) with L = Him (**2**), Htrz (**6**), and Hind (**8**) in DMF against their corresponding redox potentials is depicted in Figure 14. The plot, expressed by eq 5, provides a reasonable fit, although the influence of other, yet unknown, contributing factors cannot be ruled out.

$$\log k\ (s^{-1}) = -4.280E_{1/2}[Ru^{III/II}] - 0.647 \quad (r = 0.93) \tag{5}$$

In fact, the triazole-based complexes **B4** and **B6** are more inert than expected, as well as the positively charged complexes **C2** and **C3**, whose cathodically induced solvolysis is only detected upon CPE (see above). Generally, k_1 does not differ significantly in DMSO or DMF, but k_2 does differ considerably, indicating that the S-bonded DMSO ligand makes the reduced complex more inert than the DMF ligand (Table 6), in agreement with the increased lability of *trans*-$[RuCl_4L_2]^-$ (**A**) compared to *trans*-$[RuCl_4L(DMSO)]^-$ toward Cl^- ligand displacement by DMF upon reduction.[6]

In the case of *trans*-$[RuCl(NH_3)_4(Y)]^{2+}$, where Y is pyridine, isonicotinamide, or acetonitrile, the π-acceptor ligands have been shown to slow halide aquation reactions upon reduction, which was attributed to an increased effective charge on the Ru^{II} ion.[41]

(41) Marchant, J. A.; Matsubara, T.; Ford, P. C. *Inorg. Chem.* **1977**, *16*, 2160−2165.

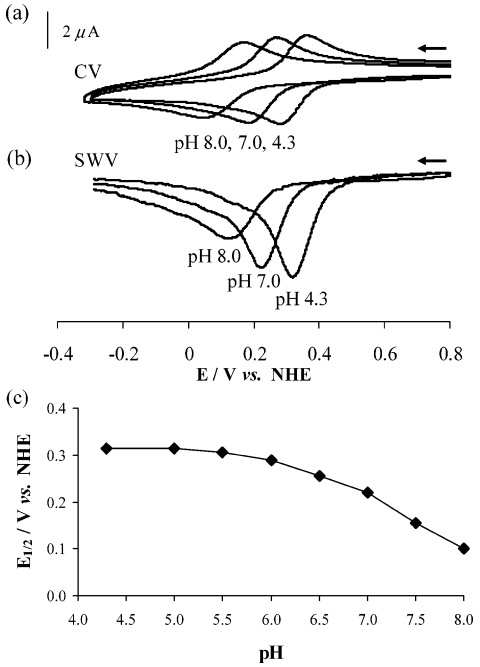

Figure 15. Cyclic voltammograms (a, 0.20 V s^{-1}) and square wave voltammograms (b, 2 mV step height, 25 mV pulse, 100 Hz frequency) of 2.0 mM *trans*-$[RuCl_2(Htrz)_4]Cl$ (**C6**) in 0.2 M phosphate buffer at different pH values. (c) The Ru^{III}/Ru^{II} half wave potential as a function of pH (Pourbaix plot) for *trans*-$[RuCl_2(Htrz)_4]Cl$ (**C6**). The experimentally obtained (♦) pH-dependent $E_{1/2}$ values (in V vs NHE) are as follows (pH value of the electrolyte solution indicated in brackets): 0.315 (4.3), 0.315 (5.0), 0.305 (5.5), 0.290 (6.0), 0.255 (6.5), 0.220 (7.0), 0.155 (7.5), 0.10 (8.0).

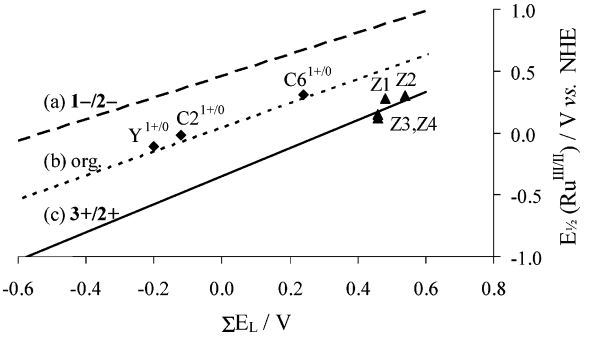

Figure 16. Plot of $E_{1/2}$ (I^{red}) in aqueous medium against $\sum E_L$ (in V vs NHE) for the $Ru^{III} \rightarrow Ru^{II}$ reduction process of net 1+ charged complexes (♦) **C2** ($E_{1/2} = -0.02$ V at pH = 7.0, 0.2 M phosphate buffer), **C6** ($E_{1/2} = 0.32$ V at pH < 5, 0.2 M phosphate buffer), and *cis*-$[RuCl_2(NH_3)_4]Cl$ (**Y**, 1 M $NaClO_4$, $E_{1/2} = -0.11$ V,[42] $\sum E_L = -0.20$ V[35]). In addition, the imidazole-based complexes involving net 3+ and 2+ charged species (▲) $[Ru^{II}(1meim)_6]Cl_2$ (**Z1**, $E_{1/2} = 0.28$ V,[34] $\sum E_L = 0.48$ V[35]), $[Ru^{III}(Him)_6](ClO_4)_3$ (**Z2**, $E_{1/2} = 0.30$ V,[34] $\sum E_L = 0.54$ V[35]), *trans*- (**Z3**, $E_{1/2} = 0.12$ V,[34] $\sum E_L = 0.46$ V[35]) and *cis*-$[Ru(NH_3)_4(Him)_2]Cl_3$ (**Z4**, $E_{1/2} = 0.15$ V,[34] $\sum E_L = 0.46$ V[35]) are indicated. The general linear relationship for the $Ru^{II} \rightarrow Ru^{III}$ oxidation in water for 2+ (c, solid line), the $Ru^{III} \rightarrow Ru^{II}$ reduction in 0.2 M phosphate buffer at pH 7.0 for 1− charged (a, dashed line) complexes (refs 35 and 6, respectively), and the correlation established for the prediction of $E_{1/2}$ (Ru^{III}/Ru^{II}) in organic solvents (b, dotted line) are also displayed.

Aqueous Medium. In the 0.20 M phosphate buffer at pH 7.0, complexes **C2** and **C6** (the only complexes sufficiently soluble in this medium) are stable within at least 3 h at room temperature showing negligible spectral changes (Figure S8). The electrochemical behavior of the **A** complexes in aqueous medium was studied previously by CV.[6] These exhibit one Ru^{III}/Ru^{II} reduction wave at −0.16−0.03 V vs NHE in 0.2 M phosphate buffer at pH 7.0. The cyclic and square wave voltammograms of complexes **C2** and **C6** in the same medium (pH 7.0) display one reversible single-electron $Ru^{III} \rightarrow Ru^{II}$ reduction wave at −0.02 and 0.22 V vs NHE for **C2** and **C6**, respectively. Both Ru^{III}/Ru^{II} redox potentials are biologically available in vivo. The monopositively charged complex *cis*-$[Ru^{III}Cl_2(NH_3)_4]^+$ (**Y**) was reported to be reduced at a slightly lower redox potential: −0.11 V vs NHE.[42]

The pH dependence of the electrochemical behavior of complexes **C2** and **C6** was investigated by cyclic voltammetry and square wave voltammetry. While the redox potential of **C2** was not affected by variation of the pH of the electrolyte solution between pH 5.0 and 7.5 (all measured redox potentials were between −0.015 and −0.025 V vs NHE), complex **C6** shows a pH-dependent electrochemical response around neutral pH values (Figure 15). The Ru^{III}/Ru^{II} redox potential of **C6** was pH independent at pH < 5, and showed a pH-dependent slope of −0.06 V/pH at pH 6.0−6.5 (indicative of an one electron/one proton couple in accordance with the Nernst equation) and of −0.12 V/pH (one electron/two proton couple) around pH 7.5. As expected for redox-active pH responsive molecules, the oxidized form of **C6** is less basic than the reduced one because of the stronger electron-withdrawing properties of the Ru^{III} metal center compared to that of Ru^{II}. The pH-independent electrochemical behavior of **C2** is explained by the higher pK_a value of the imidazole compared to that of the 1,2,4-triazole (14.4 and 10.0,[36] respectively, for the free azole ligands). The pH-dependent redox potentials for the imidazole complex could only be expected at pH > 7.5.

Two sets of parameters are known[6,35] to predict (by using the general eq 1) the redox potentials for the Ru^{III}/Ru^{II} redox couple in aqueous medium: $S_M = 1.14$, $I_M = -0.35$ V for the oxidation of Ru^{II} to Ru^{III} (involving the 2+ and 3+ charged species)[35] and $S_M = 0.88$, $I_M = 0.46$ V for the reduction of Ru^{III} of net 1− charged complexes to the 2− charged Ru^{II} species (in 0.2 M phosphate buffer at pH 7.0 by using azole-based ruthenium complexes).[6] The **C** complexes and *cis*-$[RuCl_2(NH_3)_4]Cl$ (**Y**) exhibit a net 1+/0 net charge in the metal(III/II) oxidation states, and the redox potential values for their Ru^{III}/Ru^{II} reduction lie between those predicted for complexes involving net 3+/2+ and 1−/2− charged species in their Ru^{III}/Ru^{II} redox process (Figure 16, including reported redox potentials of net 3+ and 2+ charged imidazole-based ruthenium complexes).

The redox potential reflects the relative free energies of both the oxidized and reduced species. While in organic solvents the S_M and I_M values of a given redox couple are generally insensitive to the net charge of the species[35] (concomitant with a negligible difference in solvation energy for both species), they appear to be largely affected in water by a significant net charge dependent hydration. For the ruthenium complexes studied (Figure 16), an increasing complex net charge results in a lower redox potential.

(42) Yee, E. L.; Cave, R. J.; Guyer, K. L.; Tyma, P. D.; Weaver, M. J. *J. Am. Chem. Soc.* **1979**, *101*, 1131−1137.

This observation may be, in part, explained by the electrostatic Born model, which shows that the negative Gibbs energy of hydration of a given ion is a function of the squared net charge z ($-\Delta G^{hydr} = \text{const}\cdot z^2$).[43] Thus, the more positive the difference of the squared charge for the reduced minus the oxidized species ($z_{red}^2 - z_{ox}^2$), the more stable the hydrolyzed reduced (compared to the oxidized) species and consequently the higher the Ru^{III}/Ru^{II} redox potential. It should be noted that the Ru^{III}/Ru^{II} redox potential values of the low-charged complexes **C2** and **C6** (involving 1+/0 net charged species) are only slightly more positive than those predicted by using Lever's approach and the S_M and I_M parameters for organic solvents [$\Delta E(^{aq}E_{1/2}^{obs} - {}^{org}E_{1/2}^{pred}) = 0.06$ and 0.05 V (pH < 5), respectively]. This might be explained by a small difference between the values of squared charges for the oxidized and reduced species, suggesting that the organic S_M and I_M values might be suitable to give a reasonable estimate of the Ru^{III}/Ru^{II} redox potentials of low charged ruthenium complexes in aqueous medium.

Figure 16 shows that the indicated slopes, S_M, in water are not largely affected by variation of the complex net charge. Thus, the ligand sensitivity of the oxidized (Ru^{III}) compared to the reduced (Ru^{II}) species seems to be little dependent on the net charge. In addition, the intercept I_M is dependent on the difference of the solvation energies of a given redox couple,[35] in agreement with the observed net charge-dependent intercepts.

Although these observations on the electrochemical net charge dependence in aqueous medium appear to be of much importance, they require further investigations of different net charges to test for their generality.

Final Remarks

The encouraging results in phase I clinical trials of (H_2ind)[*trans*-$RuCl_4$(Hind)$_2$] and the recent discovery that the replacement of the chloro ligands with indazole ligands enhances the antiproliferative activity demanded the synthesis and characterization of further derivatives with the aim to establish useful structure−property relationships. A linear correlation of the ligand electrochemical parameters, E_L, of azole ligands and their corresponding basicity (pK_a of the azolium ion) allows the prediction of the E_L values for other azole heterocycles with known pK_a values. In addition, a logarithmic correlation between the kinetic rate constants of the reductively induced solvolysis in DMF and the redox potential for the Ru^{III}/Ru^{II} redox couple containing azole and chloro ligands was found, which demonstrates that an increase of the net electron-donor character (decrease of E_L) of the ligands and of the basicity (increase of pK_a of the corresponding free azolium acid H_2L^+) of the azole ligand promotes the complex lability toward the solvolytic dechlorination upon reduction and shifts the $Ru^{III} \rightarrow Ru^{II}$ redox potential cathodically.

The first water soluble complexes of the general formula [$RuCl_2$(azole)$_4$]Cl are reported. They do not undergo ligand exchange reactions within several hours in 0.2 M phosphate buffer at pH 7.0 at room temperature, an important aspect for a drug candidate.

While a pronounced anodic shift of the reduction potential in organic media is observed when chloro ligands are replaced by azole ligands, an unexpected small increase of the complex redox potential is detected in aqueous phosphate buffer. The redox potentials of **C2** and **C6** are similar to those of Na[*trans*-$RuCl_4$(Hind)$_2$] [KP1339, $E_{1/2}(Ru^{III}/Ru^{II}) = 0.03$ V] and (H_2im)[*trans*-$RuCl_4$(Him)(DMSO)] [NAMI-A, $E_{1/2}(Ru^{III}/Ru^{II}) = 0.25$ V vs NHE in 0.2 M aqueous phosphate buffer at pH 7.0],[6,7] for which an in vivo reduction is supposed.[5] The small anodic shift of the redox potential on the replacement of the anionic chloro ligand by the neutral azole ligands is surprising because both less electron-donating ligands and a higher complex charge are expected to increase the redox potential. This behavior is however explained by the net charge-dependent Gibbs energy of hydration as described in the Born model.

In addition, while the redox potential of **C2** is pH independent around neutral pH, complex **C6** shows a pH-dependent redox potential at physiologically relevant pH values. This makes triazole-based ruthenium complexes interesting for the future preparation of bioreductive prodrugs activated by reduction in the acidic extracellular environment of the hypoxic tumor tissue, although the pH-dependent redox response of biologically relevant reducing agents has to be taken into account.

The findings described should be considered in the future design of ruthenium pharmaceuticals to successfully predict the Ru^{III}/Ru^{II} redox properties, although the generality of some of the above conclusions has still to be tested with a wider variety of ruthenium complexes.

Acknowledgment. The authors are indebted to FWF (Austrian Science Fund), University of Vienna (International Relations Office), the Foundation for Science and Technology and its POCTI-program (FEDER funded) (Portugal), and the European Community (contract MRTN-CT-2003-503864) for financial support. Prof. V. Yu. Kukushkin is acknowledged for stimulating discussions and support in the preparative part of the work, Dr. Ch. Hartinger and Dr. A. Nazarov for their assistance with mass spectrometry investigations, and Dr. M. Galanski for NMR measurements.

Supporting Information Available: X-ray crystallographic files in CIF format for **B1**, **B4**−**B7**, **C2**, **C3**·CH_3OH·$(C_2H_5)_2O$, **C6a**·$2H_2O$, **C7**, and **E4b** and additional tables, figures, and a description of crystal structures. This material is available free of charge via the Internet at http://pubs.acs.org.

IC0503737

(43) Born, M. *Z. Phys*. **1920**, *1*, 45−48.